H11 meltwater and standard 127ka Last Interglacial simulations suggest more modest peak temperatures for both Greenland and Antarctica: A multi-model study of water isotopes

Louise C. Sime[1], Rahul Sivankutty[1], Irene Malmierca-Vallet[1], Sentia Goursaud Oger[2,1], Allegra N. LeGrande[3], Erin L. McClymont[4], Agatha de Boer[5], Alexandre Cauquoin[6], and Martin Werner[7]

[1]Ice Dynamics and Paleoclimate, British Antarctic Survey, Cambridge, United Kingdom
[2]CEA, DAM, DIF, F-91297 Arpajon, France
[3]NASA Goddard Institute for Space Studies, New York, USA
[4]Department of Geography, Durham University, Durham, UK
[5]Department of Geological Sciences, Stockholm University, Stockholm, Sweden
[6]Institute of Industrial Science, The University of Tokyo, Kashiwa, Japan
[7]Alfred Wegener Institute, Helmholtz Centre for Polar and Marine Research, Bremerhaven, Germany

Correspondence: Louise C. Sime (lsim@bas.ac.uk)

Abstract. The Last Interglacial (LIG) period, approximately 130,000 to 115,000 years ago, represents one of the warmest intervals of the past 800,000 years. Here, we simulate water isotopes in precipitation over Antarctica and the Arctic during the LIG, using three isotope-enabled atmosphere–ocean coupled climate models: HadCM3, MPI-ESM-wiso, and GISS-E2.1. These models were run following the Paleoclimate Modelling Intercomparison Project phase 4 (PMIP4) protocol for the LIG at 127 ka (kilo-years ago), supplemented by a 3,000-year Heinrich Stadial 11 (H11) experiment using HadCM3. The long H11 simulation applies Northern Hemisphere meltwater to the North Atlantic, causing large-scale changes in ocean circulation—including cooling in the North Atlantic and Arctic, and warming in the Southern and Global Oceans. While the standard 127 ka simulations do not capture the observed Antarctic warming and sea ice reduction in the Southern Ocean and Antarctic regions, they do capture around half of the warming in the Arctic. The H11 simulations align more closely with observations than the 127 ka simulations. H11 captures more than 80% of the warming, sea ice loss, and $\delta^{18}O$ changes for both Greenland and Antarctica. Decomposition of seasonal $\delta^{18}O$ drivers highlights the dominant role of sea-ice retreat and associated changes in precipitation seasonality in influencing isotopic values across all simulations, alongside a smaller common response to orbital forcing. We use the H11 and multi-model 127 ka simulations together to infer LIG surface air temperature (SAT) changes based on ice core measurements. The peak inferred LIG Greenland SAT increase is $+2.89 \pm 1.32$ K at the NEEM ice core site—less than half the previously inferred warming. Peak inferred LIG Antarctic SAT increases are $+4.39 \pm 1.45$ K at EDC, dropping to $+1.67 \pm 3.67$ K at TALDICE. These calculated warming values reflect climate effects alone and do not account for any ice flow or site elevation–related impacts. Coastal sites in Greenland and Antarctica appear to have experienced less warming compared with higher central regions.

1 Introduction

The Last Interglacial (LIG) period, or Eemian, occurring approximately 130,000 to 115,000 years ago, stands out as one of the warmest interglacials in paleoclimate records over the past 800 thousand years (Past Interglacials Working Group of PAGES, 2016). The globe experienced temperatures higher than preindustrial levels during peak LIG conditions (Hoffman et al., 2017; Fischer et al., 2018). Estimates of global mean maximum surface air temperature LIG warming of 0.8±0.5K above pre-industrial levels are supported by Hoffman et al. (2017), Fischer et al. (2018), and Shackleton et al. (2020). The magnitude of warming was greater in polar and subpolar regions compared to the global-mean value (CAPE-Last Interglacial Project Members, 2006; Sime et al., 2009; Capron et al., 2014, 2017). Sime et al. (2023) estimated the Arctic wide summer surface air temperature warming at 127 ka to be 3.7± 1.5K, when the Arctic may have been sea ice free during summer (Guarino et al., 2020; Vermassen et al., 2023); whilst Greenland surface temperatures as high as 8 ± 4 K warmer than the PI has been posited by NEEM community members (2013). Similarly, peak LIG annual mean warming over central Antarctic ice core sites of +3-6 K have been suggested (*e.g.* Jouzel et al., 2007; Sime et al., 2009; Otto-Bliesner et al., 2013; Bakker et al., 2014; Capron et al., 2014).

Alongside the increases in polar surface air temperatures, sea ice cover was reduced and sea surface temperature warmed across the Arctic and Southern Oceans at 127-128 ka compared to the preindustrial period (Holloway et al., 2017; Chadwick et al., 2023). Recently Vermassen et al. (2023) used open water species, found in Arctic marine cores, to suggest that the Arctic was likely seasonally sea ice-free during the LIG, though Arctic age models are currently characterized by significant uncertainty (Razmjooei et al., 2023). This supports the idea that sea ice feedbacks were important in amplifying the Arctic LIG warming (Guarino et al., 2020; Diamond et al., 2021, 2023). In the Southern Ocean work on diatom fossil assemblages in marine sediment cores and sea-salt sodium in Antarctic ice cores helps underpin our understanding of Antarctic sea ice (Wolff et al., 2006; Crosta et al., 2022; Chadwick et al., 2020, 2021, 2022). Gao et al. (2024a) examined four recent Southern Ocean core syntheses (from: Capron et al., 2017; Hoffman et al., 2017; Chandler and Langebroek, 2021; Chadwick et al., 2021), and estimated a Southern Ocean annual SST anomaly of around +1.3K at 127 ka.

Whilst the Arctic summer warmth and loss of sea ice during the LIG can be attributed mainly to orbital forcing (Guarino et al., 2020; Diamond et al., 2023; Sime et al., 2023; Vermassen et al., 2023), the reduced sea ice and warmer Southern Ocean is not attributable to either orbital or greenhouse gas forcing, as austral summer solar insolation was lower, and greenhouse gas concentrations were below preindustrial levels at 127 ka (Berger and Loutre, 1991; Otto-Bliesner et al., 2017). Although the Antarctic ice sheet volume and configuration remain poorly constrained (Golledge et al., 2021), modelling studies nevertheless show that a smaller than preindustial ice sheet alone is very unlikely to account for the estimated LIG sea ice loss and Southern Ocean warming (Holloway et al., 2016; Hutchinson et al., 2024). Alongside this, recent simulations run according to standard Paleoclimate Modelling Intercomparison Project (PMIP) LIG protocol (Otto-Bliesner et al., 2017), which applies 127 ka orbital and greenhouse gas forcing, also do not fully replicate the pronounced warmth at southern mid-to-high latitudes (Lunt et al.,

2013; Otto-Bliesner et al., 2017, 2021; Kageyama et al., 2021). This model-observation mismatch may be due to the models not capturing a prolonged period of meltwater influx from the Northern Hemisphere ice sheet melt, and subsequent weakening of the Atlantic Meridional Overturning circulation with warming of the south due to the bipolar seesaw effect (Holloway et al., 2018; Sime et al., 2019a; Chadwick et al., 2023; Gao et al., 2024a).

From approximately 132 to 128 ka, in the period before peak LIG warmth, meltwater entered the North Atlantic from the deglaciation of the large Northern Hemisphere glacial-period ice sheets. The event is sometimes called Heinrich 11 (H11), although technically a Heinrich event is defined as the occurrence of very significant meltwater markers (*e.g.* ice-rafted debris) in North Atlantic sediment cores (Heinrich, 1988; Hemming, 2004), rather than being a simple label for the period marked by Northern Hemisphere meltwater entering the oceans. The extra freshwater reduced the thermohaline circulation-driven part of the Atlantic Meridional Overturning Circulation (AMOC), and decreased the associated export and loss of global heat through and to the North Atlantic (Rahmstorf, 2000; Weaver et al., 2003; Clark et al., 2002; McManus et al., 2004). This resulted in large-scale changes in ocean circulation, including cooling in the North Atlantic and Arctic, and warming in the Southern and Global Ocean. Recent dating of the H11 event suggest that the meltwater could have persisted for 3000 to 5000 years (length partly depending on definition of 'Heinrich') and that it is possible that the meltwater ceased directly before peak LIG temperatures at both poles (Marino et al., 2015; Stoll et al., 2022).

Given the progress in understanding the processes key to Last Interglacial (LIG) climate at the poles, it seems timely to revisit the question of inferring, or quantifying, polar warming during the LIG from ice core measurements. Ice core stable water isotopes ($\delta^{18}O$) from Antarctica and Greenland provide invaluable information on past variations in site temperature (EPICA community members, 2004; Jouzel et al., 2007; Sime et al., 2013; Malmierca-Vallet et al., 2018; Domingo et al., 2020). Jouzel et al. (1997) note that linear relationships between the mean annual $\delta^{18}O$ content in precipitation and the mean annual temperature at the precipitation site in polar regions support this use of ice core measurements. However, retrieving accurate LIG peak temperature information from $\delta^{18}O$ values is challenging (*e.g.* Jouzel et al., 1997, 2003; NEEM community members, 2013; Goursaud et al., 2021). In particular, temporal slopes often appear lower than present-day spatial slopes (Jouzel et al., 1997; Guan et al., 2016).

The most important local-site control on $\delta^{18}O$ in polar precipitation is thought to be the site condensation temperature (Dansgaard, 1954; Jouzel et al., 1997). Lee et al. (2008) and Liu et al. (2023) therefore examine relationships between condensation temperature and inversion layers in Antarctica, and the reconciliation of spatial and seasonal $\delta^{18}O$–temperature relationships, finding relationships of around 1.2‰/K between inversion layer and $\delta^{18}O$ in precipitation.

Additional local-to-regional influences include changes in local boundary layer conditions (*e.g.* Krinner et al., 1997; Noone and Simmonds, 2002) and the impacts of continental vapor recycling (*e.g.* Werner et al., 2001; Sjolte et al., 2014).

However, $\delta^{18}O$ is also dependent on the origin of the vapour and its associated pathways and history as it travels to the precipitation site (Dansgaard, 1954; Boyle, 1997; Kindler et al., 2014; Guan et al., 2016). Changes in Greenland $\delta^{18}O$ during climate shifts have been shown to be sensitive to both source properties and pathway changes (Boyle, 1997; Werner and Heimann, 2002), along with key controls such as precipitation seasonality and intermittency. These factors affect Antarctica

and Greenland differently due to the nature of precipitation, sea ice, and other geographically specific influences (Werner et al., 2001; Sime et al., 2008, 2013; Münch et al., 2020).

For example, Vinther et al. (2010); Sjolte et al. (2014) show that local temperature controls on Greenland $\delta^{18}O$ can be weak during summer; this may be partially due to the limited impact of sea ice in summer (*e.g.* Sime et al., 2013; Sjolte et al., 2014; Sime et al., 2019b). Many recent studies now consider such factors, including air mass trajectories and vapour-to-precipitation distance (*e.g.* Delaygue et al., 2000; Schlosser et al., 2004), evaporation and ocean surface conditions (*e.g.* Vimeux et al., 1999), and especially sea ice (*e.g.* Bertler et al., 2018; Holloway et al., 2016, 2017).

Seminal work by Petit et al. (1999) at Vostok in Antarctica used a $\delta^{18}O$–temperature relationship of 0.7‰/K, while in West Antarctica, WAIS Divide Project Members (2015) used a relationship of 0.8‰/K. For Greenland, at the NEEM core site, NEEM community members (2013) used a value of 0.48 ± 0.1‰/K.

However, given the timescale, regional, and climate-shift-dependent controls on $\delta^{18}O$ across Antarctica and Greenland, it is imperative to study the relationships between $\delta^{18}O$ and temperature for each specific climate shift, especially where we seek to infer temperature from measured changes in $\delta^{18}O$ in ice cores (Jouzel et al., 1997).

Isotope-enabled General Circulation Models (GCMs) allow a more direct comparison of model isotopic outputs with water isotope concentrations measured in natural archives, including ice cores. These models provide the most comprehensive means that we possess to include all the factors that affect the $\delta^{18}O$ and surface air temperature changes (Werner et al., 2001; Werner and Heimann, 2002). They have therefore been used to investigate $\delta^{18}O$ and temperature in polar regions, and to provide a theoretical framework that accounts for both spatial and temporal variations in isotopic signals (Werner and Heimann, 2002; Sime et al., 2008). This study investigates water isotope changes in precipitation in the Antarctic and the Arctic regions that occurred between the PI and LIG using three isotope-enabled GCMs, and is the first isotopic-enabled multi-model study of the LIG. LIG simulations are run with each of these models according to the recent PMIP4 LIG protocol (Otto-Bliesner et al., 2017). These simulations are supplemented by a long 3000-year H11 experiment which is run using HadCM3. The Methods section (2) details these models, experimental set-ups, and ice core $\delta^{18}O$ and climate data, alongside analysis methods. Section 3 presents the results, Section 4 discusses the findings, and Section 5 concludes the study.

2 Methods

The Methods section details: the three water-isotope enabled models used; simulations run with these models; how model output is handled and analysed; and Antarctic and Greenland ice core $\delta^{18}O$ and wider set of observations used to evaluate the model simulations.

2.1 Models

The use of three isotope-enabled models aids in understanding model-dependency of results. The models are: the Max Planck Institute for Meteorology Earth System Model here referred to here as MPI-ESM-wiso (Cauquoin et al., 2019); the Goddard Institute for Space Studies coupled ocean-atmosphere model: GISS-E2.1-G (Kelley et al., 2020); and version 4.5 of the Hadley

Table 1. Simulation names, models versions, and boundary conditions. Note all simulations are run with a pre-industrial ice sheet configuration. The magnitude of the H11 freshwater forcing is 0.25 Sverdrups. See also Sections 2.1 and 2.2.

Simulation name	Model (and version)	Orbital forcing	GHG forcing	Spin-up (years)	Duration of H11 forcing
$ECHAM6_{PI}$	ECHAM6 (MPI-ESM-wiso)	1850 C.E	(CO_2=284 ppm, CH_4=808 ppb N_2O=273 ppb)	3500	-
$GISS_{PI}$	GISS (ModelE2.1-G)			1000	-
$HadCM3_{PI}$	HadCM3 (UM4.5)			2000	-
$ECHAM6_{127k}$	ECHAM6 (MPI-ESM-wiso)	127ka	(CO_2=275 ppm, CH_4=685 ppb, N_2O=255 ppb)	2800	-
$GISS_{127k}$	GISS (ModelE2.1-G)			1000	-
$HadCM3_{127k}$	HadCM3 (UM4.5)			2000	-
H11-200	HadCM3 (UM4.5)	128ka	(CO_2=275 ppm, CH_4=705 ppb, N_2O=265 ppb)	1000	0.25Sv for 200 years
H11-3000	HadCM3 (UM4.5)			3800	0.25Sv for 3000 years
H11-overshoot	HadCM3 (UM4.5)			3900	0.0Sv, 200 years post-H11-3000

Centre Climate model: HadCM3 (Tindall et al., 2009). MPI-ESM (version 1.2 Giorgetta et al., 2013; Mauritsen et al., 2019) has been used for a wide range of paleoclimate simulations (*e.g.* Otto-Bliesner et al., 2021). Here we use the low resolution (LR) version, which has 1.875°×1.875° and 47 hybrid vertical levels in the atmosphere, and 1.5°×1.5° and 40 levels in the ocean component. Subsequent to the addition of water isotope module, is usually called MPI-ESM-wiso (Cauquoin et al., 2019). GISS-E2.1 is the Goddard Institute for Space Studies GISS ModelE2.1-G which has an atmospheric resolution of 2° latitude by 2.5° longitude, with 40 vertical layers up to 0.1 hPa coupled to the GISS Ocean v1 model with a resolution of 1° latitude by 1.25° longitude with 40 layers. Its vegetation uses the demographic global vegetation model called Ent Terrestrial Biosphere Model (Kelley et al., 2020). HadCM3 couples a hydrostatic atmospheric component HadAM3 and a barotropic ocean component HadOM3 (Tindall et al., 2009). The HadAM3 atmospheric model has a horizontal resolution of 2.5°×3.75° and 19 hybrid vertical levels, while the HadOM3 ocean model has a horizontal resolution of 1.25°×1.25° and 20 oceanic levels. The water isotope module of HadCM3 is described in Tindall et al. (2009).

2.2 Model simulations and output

Our series of simulations focuses on the LIG climate and isotope maximum in Antarctica and the Arctic. For each model, a pre-industrial (PI) control simulation is set-up following, or closely approximating the protocol in Eyring et al. (2016). For each model, the PI experiment is run for a period long enough to reach a pseudo-equilibrium state (*i.e.*, negligible drifts in the atmosphere, surface, and mid depth ocean). For MPI-ESM-wiso, the simulation has been continued for 2500 model years from a standard simulation without isotopes, which was run for 1000 years (so 3500 years in total) (Cauquoin et al., 2019). For GISS the pre-industrial simulation is begun from WOA observed conditions with isotopic composition of the whole ocean prescribed, and then spun-up for 1000 years, with the last 100 years used in this study. For HadCM3, the PI spin-up is more

than 2000 years in length. Previous evaluation of each model against observations suggests that the simulated distribution of isotopes in polar precipitation compare well to present-day (*e.g.* Sime et al., 2008; Cauquoin et al., 2019; Oger et al., 2023).

As well as the PI control, for each model one LIG simulation is run, based on the Otto-Bliesner et al. (2017) Tier 1 lig127k protocol. The protocol specifies orbital and greenhouse gas concentrations fixed at 127-ka values (see Table 1). Atmospheric greenhouse gas concentrations are derived from ice core records at 127 ka (Otto-Bliesner et al., 2017), and use a CO_2 value of 275ppm. As specified in the protocol, sea level and ice sheet configurations are kept same as PI set-up for each model (Table 1). For MPI-ESM-wiso, the simulation has been continued for 1500 model years from a standard simulation without isotopes, which was run for 1300 years (so 2800 years in total), starting from PI state for the isotopic spatial distribution in the ocean. For GISS, the LIG simulation has the same spin-up as for the PI. And for HadCM3, it was spun-up for 1000 years, starting from a spun-up PI. These long spin-ups mean that all simulations have reached pseudo-equilibrium states, as achieved for the PI simulation. As in Table 1, these simulations are referred to using the convention $\mathrm{MODEL}_{\mathrm{TIMESLICE}}$, for example, $\text{MPI-ESM-wiso}_{\mathrm{PI}}$ and $\mathrm{GISS}_{\mathrm{127k}}$.

In addition to the primary multi-model 127k simulations, we use HadCM3 to run a Heinrich Stadial 11, or H11, simulation which directly extends the Holloway et al. (2018) simulation. This enables exploration of the effects of the Heinrich 11 (or Termination 2) ice sheet melt event, which preceded 127 ka, and how the associated meltwater entering the North Atlantic on climate, and associated $\delta^{18}O$ changes. The H11 simulation is run on from a 128 ka simulation, spun-up for the orbital and GHG conditions of 128ka over 800 years. Our Holloway et al. (2018) H11 experiment has orbital and GHG forcing that are for 128ka rather than 127ka. Gao et al. (2024a) shows that standard 127-ka and 128-ka HadCM3 simulations give very similar results: orbital changes between 127 and 128ka are slight; whereas the impacts of the meltwater forcing are large. Our H11 simulation continues to apply the same 128 ka orbital and GHG conditions, with the addition of meltwater, via standard hosing-type set-up, to the North Atlantic. In support of this variant, Otto-Bliesner et al. (2017) introduced a Tier 2 sensitivity experiment, which similarly includes a prescribed meltwater flux to the North Atlantic. Since Holloway et al. (2018); Guarino et al. (2023); Gao et al. (2024a) suggest that 3000 years of this meltwater forcing is required to allow the impacts of northern hemisphere ice sheet melt on LIG climate to fully manifest in the Southern Ocean and Antarctica, 0.25Sv of melt water is added uniformly to the surface North Atlantic Ocean between 45°and 70°N for 3100 years.

The meltwater forcing is then stopped, and an additional simulation is branched off at 3000 years, where orbital and GHG forcing continued to be applied but no further meltwater is added. This extra branch is useful to capture the initial effects of post H11 recovery, sometimes referred to as the AMOC overshoot. As in Table 1, these simulations are referred to as H11-TIME/BRANCH.

The H11 simulation represents a significantly longer meltwater forcing than previous LIG simulations run with the HadCM3 model (Stone et al., 2016; Holloway et al., 2018). Given the actual meltwater isotopic composition from deglaciating Northern Hemisphere Ice Sheets is highly uncertain, following Holloway et al. (2018) the ocean isotopic composition for the H11 simulation is set to 0 ‰ (equivalent to present day) to ensure no negative drift in whole ocean isotopic composition. This effectively uses the assumption that by the end of Heinrich Stadial-11 sea level has reached approximately present-day values, resulting in a globally integrated ocean isotopic composition of 0 ‰.

2.2.1 Model output: calculation of anomalies

All climatologies for LIG simulations are calculated using the final 100 years of output and are compared to the PI climatologies from each individual model. For the H11 simulation, specific periods are picked out for analysis at 200 and 3000 years into H11 forcing, and post H11, or AMOC overshoot; referred to respectively as H11-200, H11-3000, and H11-overshoot (See Figure A2, Table 1). For the H11 simulation, climatology for 100 year slices from initial Phase (from years 200-300 after hosing started), final phase (year 3000-3100) and part of the overshoot phase (year 200-300, after hosing is stopped) are computed. Each simulation is summarised in Table 1. LIG - PI anomalies are generally presented using the Δ notation. So, for example, anomalies in Surface Air Temperatures (SATs) would be denoted ΔSAT and be calculated for MPI-ESM-wiso as MPI-ESM-wiso$_{127k}$-MPI-ESM-wiso$_{PI}$, or for year 3000 of the H11 simulation using [H11-3000] -[HadCM3$_{PI}$].

Bilinear interpolation in latitude–longitude space is used to extract values at the ice core locations from the gridded model output. The time mean variables [and units], or climate quantities, used for each model are: surface air temperature (SAT in K), precipitation (Precip in mm/month), sea surface temperature (SST, K), sea ice concentration (SIC in %), and sea ice area (SIA in mill. km^2). To extract model output at each site, nearest neighbour interpolation is used. Summer SST is defined as the average January-February-March SST. SIA is estimated by summing the product of Antarctic SIC and grid cell area.

All δ^{18}O values are mass-weighted and presented in parts per thousand (‰), and calculated:

$$\delta^{18}\mathrm{O} = \left(\frac{\left(\frac{^{18}\mathrm{O}}{^{16}\mathrm{O}}\right)_{sample}}{\left(\frac{^{18}\mathrm{O}}{^{16}\mathrm{O}}\right)_{standard}} - 1 \right) \times 1000 \tag{1}$$

2.2.2 Model output: δ^{18}O drivers quantifying seasonality of δ^{18}O and precipitation

To help quantify the impacts of δ^{18}O and precipitation seasonality on the δ^{18}O changes between PI and LIG, we show a simple breakdown of the drivers of $\Delta\delta^{18}$O following the method used in Holloway et al. (2016), Sime et al. (2019b), and Oger et al. (2023):

$$\Delta\delta^{18}\mathrm{O}_{seasonal} = \frac{\sum_j \delta^{18}\mathrm{O}_j^{\mathrm{LIG}} \times \mathrm{Precip}_j^{\mathrm{PI}}}{\sum_j \mathrm{Precip}_j^{\mathrm{PI}}} - \frac{\sum_J \delta^{18}\mathrm{O}_j^{\mathrm{PI}} \times \mathrm{Precip}_j^{\mathrm{PI}}}{\sum_j \mathrm{Precip}_j^{\mathrm{PI}}} \tag{2}$$

$$\Delta\mathrm{Precip}_{seasonal} = \frac{\sum_j \delta^{18}\mathrm{O}_j^{\mathrm{PI}} \times \mathrm{Precip}_j^{\mathrm{LIG}}}{\sum_j \mathrm{Precip}_j^{\mathrm{LIG}}} - \frac{\sum_j \delta^{18}\mathrm{O}_j^{\mathrm{PI}} \times \mathrm{Precip}_j^{\mathrm{PI}}}{\sum_j \mathrm{Precip}_j^{\mathrm{PI}}} \tag{3}$$

The summations (j) are over the 12 months of a year, using monthly climatological values.

2.2.3 Model output: uncertainties and δ^{18}O versus SAT relationships

We use linear regression to investigate the relationship between simulated $\Delta\delta^{18}$O and ΔSAT. The regression is fitted using one and two part fits. In the first case, this implies no change in SAT if there is no change in δ^{18}O, and *vice versa*, whilst in

the second case changes in SAT and $\delta^{18}O$ can be partly independent. This second case would take account of cases where, for example, there a PI-to-LIG climate change that affects only SAT or only $\delta^{18}O$, but not both. All linear regressions are performed using the ordinary least squares (OLS) method, utilizing the Python package 'statsmodels' (Seabold and Perktold, 2010), which provides robust tools for linear modeling. To quantify the uncertainties in the predicted dependent variable, confidence intervals are calculated at the 95% level. These uncertainties help in understanding the reliability of fit. This is important given there are only six data points (corresponding to six model simulations) available. This limited number of simulations (data points) inherently increases the uncertainty of the fit. Uncertainties are calculated using the standard error of the regression coefficients, which takes into account the variance of the residuals and the distribution of the independent variable.

2.3 Arctic and Antarctic ice core $\delta^{18}O$ data

Ice core data for the LIG is available from both Greenland (Arctic) and Antarctica. LIG ice layers have been found in deep Greenland ice cores. Although dating these layers presents challenges and some may be missing, Domingo et al. (2020) inferred the "most likely" LIG peak $\delta^{18}O$ values along with the associated uncertainty ranges from six deep ice cores (Figure A1). These are: NEEM (NEEM community members, 2013); NGRIP (Members, North Greenland Ice Core Project, 2004); GRIP (Landais et al., 2003); GISP2 (Suwa and Bender, 2008; Yau et al., 2016); Camp Century (Johnsen et al., 2001); and DYE3 (Johnsen et al., 2001). These data are re-used in this study (Table A1, first four columns upper half).

Goursaud et al. (2021) presented data from six published East Antarctic ice core records that provide $\delta^{18}O$ measurements from the PI and LIG (Table A1, first four columns lower half). Most of the $\delta^{18}O$ values were in practice extracted from Bazin et al. (2013) or Masson-Delmotte et al. (2011). The sites and key original references for each site (Figure A1) are: Vostok (Petit et al., 1999); Dome F (Kawamura et al., 2007); EDC (Jouzel et al., 2007); EDML (EPICA Community Members, 2006); TALDICE (Stenni et al., 2011); and Taylor (Steig et al., 2000). The observed PI value corresponds to the average over the period 1850-1900, and the LIG value corresponds to the maximum value during the LIG period (Goursaud et al., 2021). Of these cores, Taylor is least confidently dated. It receives less emphasis in the results.

2.4 Overview of Global, Arctic, and Southern Ocean LIG temperature and sea ice changes

Given sea surface conditions and global climate play a key role in setting SAT and $\delta^{18}O$ in polar regions, it is also helpful to evaluate the model simulations against global-scale observations from the LIG. An overview of these observation-sets are provided here. Hoffman et al. (2017) estimate a global annual sea surface temperature warming during the LIG of 0.5 ± 0.3K. Based largely on this estimate, Fischer et al. (2018) then estimated a global mean maximum surface air temperature LIG warming of 0.8 ± 0.5K above pre-industrial levels. This also seems to be in line with more recent estimates of LIG global mean ocean temperature warming of 1.1 ± 0.3K at 129ka, decreasing to ~0K by around 124ka (Shackleton et al., 2020). In the Arctic, Sime et al. (2023); Guarino et al. (2020) and Vermassen et al. (2023) show together that the Arctic was likely occasionally or often practically sea ice free at 127ka, *i.e.* that the total SIA in the Arctic was less than 1 mill. km^2, and that the summer ΔSAT in the Arctic was $+3.7\pm1.5$K warmer relative to the PI, north of 70N. For the Southern Ocean, sea ice at 127 ka was reduced by

40-60% over winter compared to the preindustrial (Holloway et al., 2016, 2017; Chadwick et al., 2023), and Gao et al. (2024a) alongside Capron et al. (2017); Hoffman et al. (2017); Chandler and Langebroek (2021); Chadwick et al. (2021) estimate a Southern Ocean annual SST anomaly of around +1.3°C at 127 ka relative to present.

3 Results

We first assess the global and polar sea surface changes, with a focus on summer ΔSAT and ΔSIC for the Arctic and Antarctic regions to assess whether simulations capture the observed 127ka warming. The next portion of the results considers ΔSAT, ΔPrecip, and $\Delta\delta^{18}O$ across Greenland and Antarctica, alongside an evaluation of the impact of changes in seasonality on $\Delta\delta^{18}O$. Then we use simulated $\Delta\delta^{18}O$ and ΔSAT to infer ΔSAT from $\Delta\delta^{18}O$ measured in ice cores, and to obtain estimates of the climate-related polar warming at Greenland and Antarctic ice core sites.

3.1 Model climatology: Do our simulations capture the polar and global climate of 127ka?

3.1.1 Global temperature

The 127k simulations show a small global cooling with global-mean ΔSAT from -0.23 to -0.11 K and ΔSST from -0.17 to -0.07K (Table A2). In association with this, $HadCM3_{127k}$ and $MPI\text{-}ESM\text{-}wiso_{127k}$ show a cooling of -0.016 to -0.045K in global mean ocean temperature (GMOT). The longer H11 simulations show progressive global warming during the H11 event: the H11-200, H11-3000, and H11-overshoot simulations show global-mean ΔSAT of -0.23, 0.35, and 1.09 and ΔSST of 0.04, 0.45, and 0.83 K, and ΔGMOT for the H11-3000 and H11-overshoot simulations are both +0.8K (Table A2). Thus whilst all 127k simulations show a slight global cooling, the H11 simulations (particularly the H11-3000) show warmer global SST, SAT, and GMOT changes. Towards the end of the 3000 years of H11 forcing, results from these H11 simulations match the Fischer et al. (2018) and Shackleton et al. (2020) estimates of these global quantities.

3.1.2 Arctic temperature and sea ice

Kageyama et al. (2021) and Sime et al. (2023) show that all PMIP4 127k simulations have a decrease in summer SIA between the PI and 127k. However the simulations of present day and pre-industrial Arctic SIA is very variable between models, and often does not agree with observations. This can strongly affect subsequent assessment of Arctic ΔSAT, ΔSST, and ΔSIA. We find similar results for our three 127k simulations (Figure 1).

The three 127k simulations show in the Arctic a summer ΔSAT of +1.7 to +2.7 K and a summer ΔSIA reduction of between 35-55% (Table A3). Of the three models, MPI-ESM-wiso and HadCM3 have an absolute 127k summer SIA of 1.7-2.7 mill. km^2, which is not too far from the expected LIG 127ka sea ice state (Sime et al., 2023), however, the summer ΔSAT of +1.7 to +1.8K is roughly half of the observed +3.7±1.5K warming (Sime et al., 2023; Guarino et al., 2020). Thus these simulations underestimate both actual 127k summer sea ice loss, and associated Arctic summer warming. The 127k simulation that warms the most, the GISS model, has a simulation of both PI and 127k Arctic SIA that is much too large, which makes interpretation

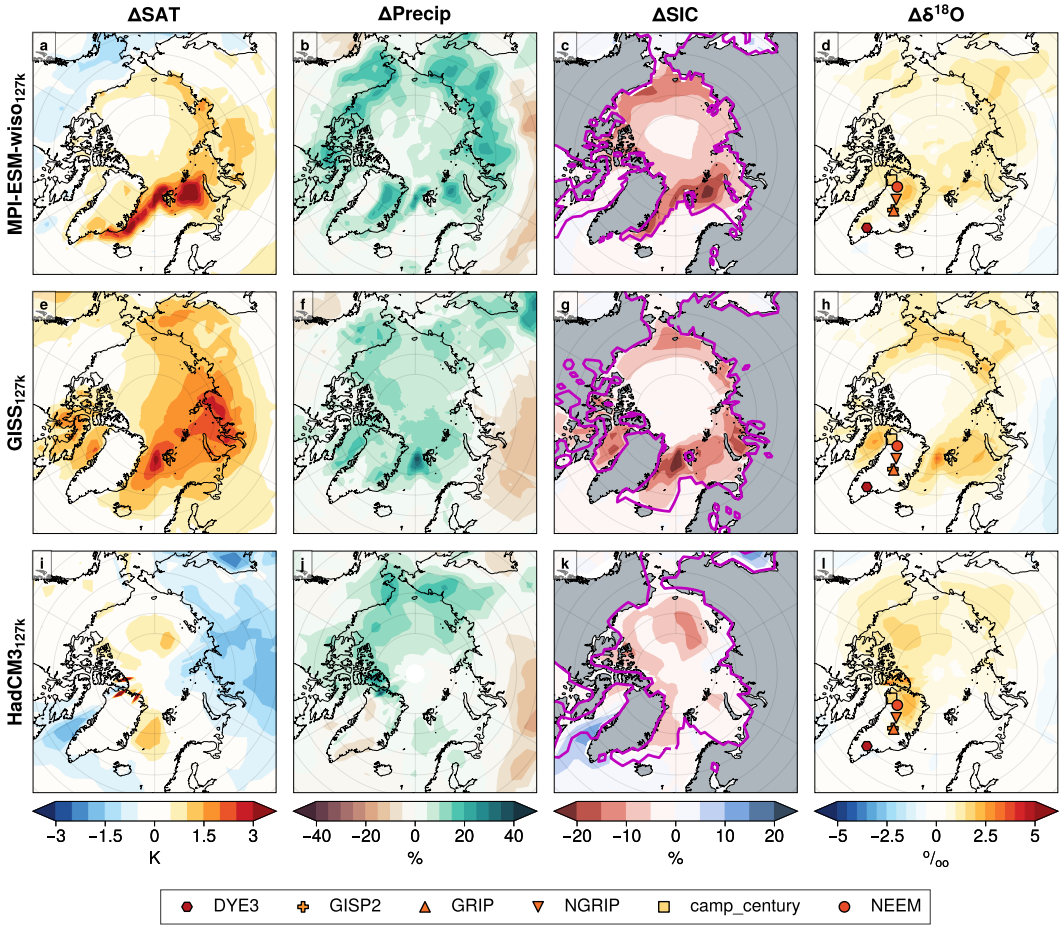

Figure 1. Anomalies in surface air temperature (ΔSAT), precipitation (ΔPrecip), sea ice concentration(ΔSIA) and $\delta^{18}O$ over Arctic region for the 127k simulations from the PI. See Table 1 for simulation details. The shaded symbols in right column shows ice core $\Delta\delta^{18}O$ values as described in Section 2.3 and Table A1. Precipitation differences are expressed as percentage deviation from mean PI values. The contours in Column 3 indicates the sea ice extent in each PI simulation.

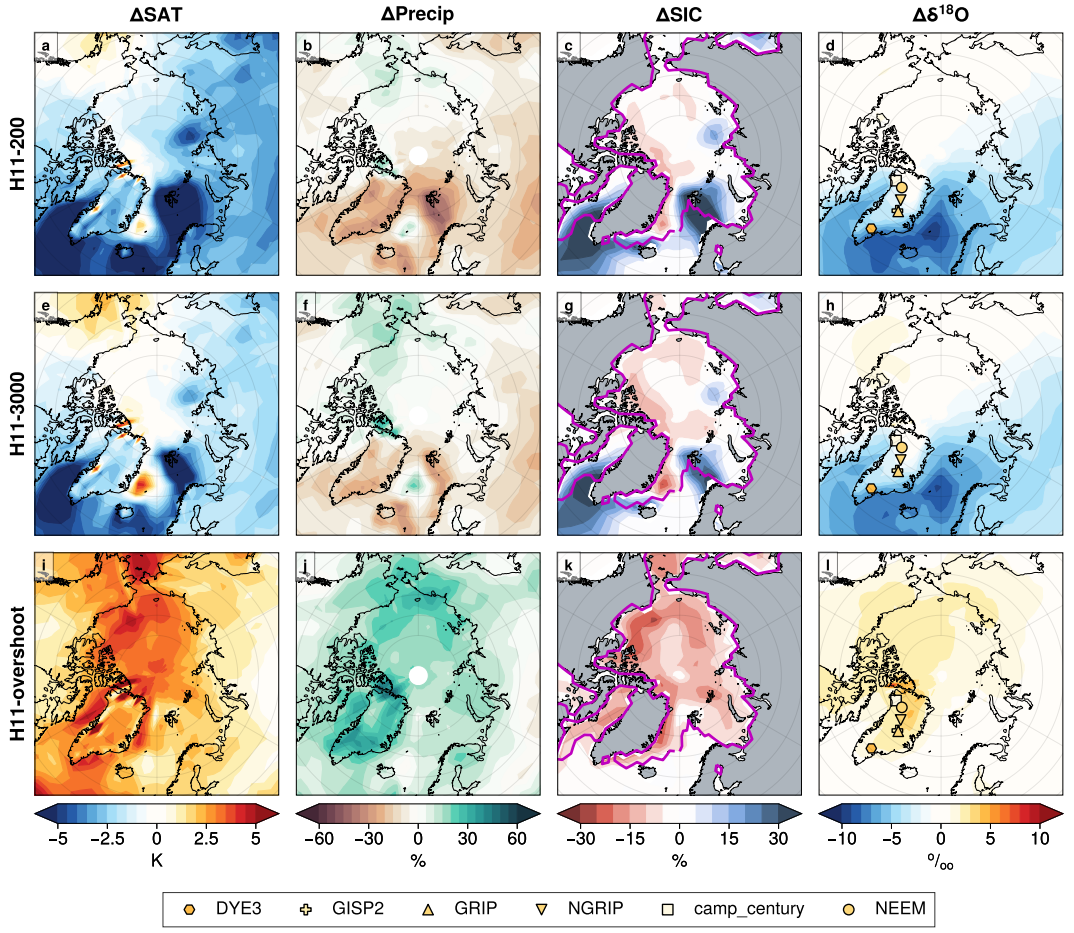

Figure 2. ΔSAT, ΔPrecip, ΔSIC and $\Delta\delta^{18}O$ over the Arctic region for the H11 simulations compared to PI; all columns and rows as for Figure 1. Note range of colorbars is wider than in Figure 1.

of the $GISS_{127k}$ Arctic changes difficult (*c.f.* Kageyama et al., 2021): effectively whilst there is a huge loss of sea ice from the LIG to the PI which drives a larger +2.7k warming of ΔSAT; 6.4 mill. km^2 remains at 127ky, which is more than five times the area of the most likely 127ky SIA (Sime et al., 2023). This vast extra area of simulated SIA strongly affects SAT, precipitation and $\delta^{18}O$, making it more difficult to draw conclusions from this particular GISS simulation. It is easier to draw conclusions from the MPI-ESM-$wiso_{127k}$ and $HadCM3_{127k}$ simulation results for the Arctic, whilst bearing in mind that these still show only half the expected summertime ΔSAT. In the case of $HadCM3_{127k}$ the too-small warming is likely partly due to the PI featuring too little ice, so that summer ΔSIA is relatively small at a 41% reduction (Table A3). For MPI-ESM-$wiso_{127k}$, the PI SIA and ΔSIA is likely a little better, but nevertheless it also shows only half of the expected summer ΔSAT (Table A3).

Of the H11 HadCM3 simulations (Figure 2), both H11-200 and H11-3000 show substantial annual mean growth of sea ice and colder sea surface and air temperatures across the Arctic and North Atlantic: Arctic annual-mean ΔSAT is -0.3K, -2.7K and

-1.5K at years 0 ($HadCM3_{127k}$), 200 (H11-200), and 3000 (H11-3000) of the H11 meltwater forcing, although due to the orbital forcing Arctic summer ΔSAT is +1.7, +0.8, and +1.2K at these years (Table A3). However, during the AMOC overshoot, the Arctic becomes very much warmer. H11-overshoot shows an Arctic annual-mean ΔSAT of +2.2K, summer ΔSAT of +3.0K, and a practically sea-ice free Arctic summer SIA of 0.7 mill. km^2, due to the rapid resumption of the AMOC and advection of warm ocean waters into the Arctic.

Thus, of our six simulations, only H11-overshoot captures the majority of the observed Arctic warming: 81% of the summer Arctic ΔSAT; a 75% loss of summer SIA; and an occasionally sea-ice free Arctic.

3.1.3 Southern Ocean and Antarctic region temperature and sea ice

Comparison against the recent synthesis in Gao et al. (2024a) allows us to ascertain the percentage of Southern Ocean ΔSST and ΔSIA captured by the simulations (Figure 3 and 4; Table A4). The three 127k simulations capture no more than 12 % of the 127ka Southern Ocean warming (Figure 5). Even MPI-ESM-$wiso_{127k}$, which shows a relatively large annual Antarctic reduction of ΔSIA of 23% and a September sea ice (winter maximum) that is reduced by 63 % (MPI-ESM-wiso generally shows the largest 127k simulation drop in all SIA quantities in both hemispheres), shows little Southern Ocean warming in association with its sea ice loss (Figure 3ab; Table A4).

In contrast, the H11-3000 simulation captures most of the warming and sea ice loss in Gao et al. (2024a) (Figure 4; Table A4). South of 40°S, annual-mean ΔSST rises by 1.3K, while reconstructed average anomalies range from +2.2K to +2.7K; summer ΔSST is 1.1K, close to 1.2-2.2K reconstructed average anomalies; September (winter) SIA reduces by 40%, similar to reconstructed 40% reduction of Southern Ocean SIC (Gao et al., 2024a). This agreement between the H11-3000 Southern and Global Ocean warming (Section 3.1.1) tends to support the idea that it is necessary to take account of the affects of the long H11 meltwater event to allow simulations to capture 127k changes in the Southern Ocean and Antarctic region (Otto-Bliesner et al., 2017; Holloway et al., 2018; Sime et al., 2019a).

Overall, the 127k simulations do not capture the observed Southern Ocean warming and sea ice loss, but the H11-3000 simulation captures between 50-100% of the warming (Table A4), depending on the particular synthesis (Gao et al., 2024a) and observation type.

3.2 Changes over the ice-sheets: ΔSAT, ΔPrecip, and $\Delta\delta^{18}O$

Having looked at how the simulations capture, or not, Global, Arctic and Southern Ocean ΔSST, ΔGMOT, ΔSAT, and ΔSIA, we now move on to look more closely at the simulation of ΔPrecip, and its associated $\Delta\delta^{18}O$ values over the Greenland and Antarctic ice sheets, with a focus on ice core locations.

3.2.1 Greenland

Most of the 127k simulation ΔSAT, ΔPrecip, and $\Delta\delta^{18}O$ changes are strongly associated with sea ice changes, including ΔSIA but also the initial (PI) sea ice state, particularly the summertime changes (Section 3.1.2; and Figure 1).

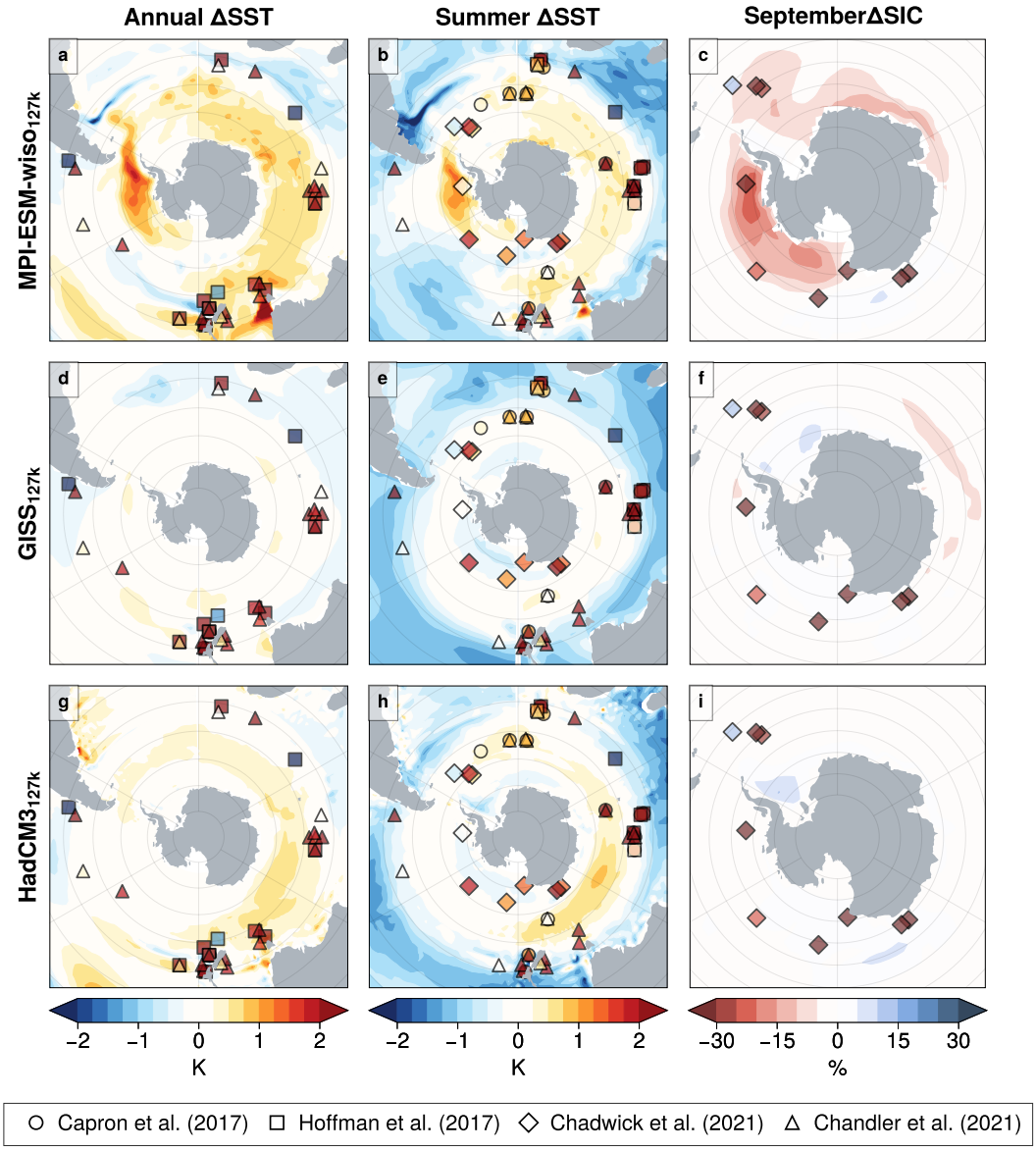

Figure 3. Reconstructed climate anomalies : (a) annual ΔSST and ΔSAT; (b) summer ΔSST; and (c) September ΔSIC over the Antarctic and Southern Ocean region for the 127k simulations compared to each PI simulation. Gao et al. (2024a) compiled these datasets from Capron et al. (2017); Hoffman et al. (2017); Chandler and Langebroek (2021); Chadwick et al. (2021).

$GISS_{127k}$ has more than 6 mill. km^2 of Arctic SIA left in the summer, meaning there is little open water or associated opportunity for proximal sea evaporation in summer. It therefore shows very little change in ΔSAT, ΔPrecip, and $\Delta\delta^{18}O$ over Greenland (Figure 1): and its Greenland core-mean $\Delta\delta^{18}O$ value is 0.0‰. In contrast, because $HadCM3_{127k}$ and MPI-ESM-

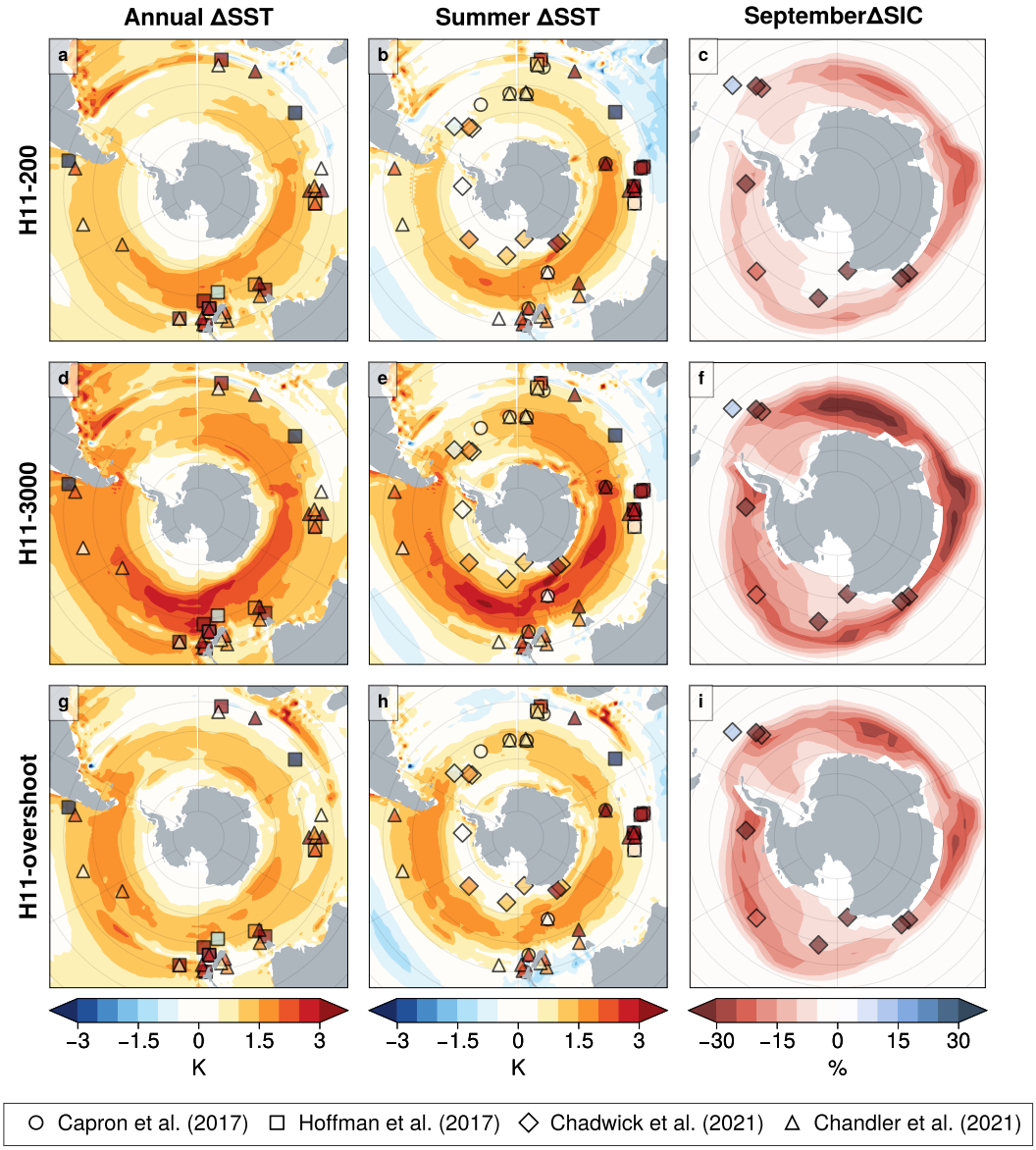

Figure 4. As Figure 3 but for the H11 simulations compared to the PI simulation.

wiso$_{127k}$ have summertime 127k SIA's of 1.7 and 2.7 mill. km^2 their $\Delta\delta^{18}$O are enriched by +0.6 ‰ and +1 ‰, respectively. This is still considerably smaller than the observed core-mean $\Delta\delta^{18}$O of +3.2‰ (Table A1). Thus the mean Arctic summertime ΔSAT is about half of the observed value, but the Greenland core-mean $\Delta\delta^{18}$O values are only one quarter to one third of the observational estimates (Domingo et al., 2020; Sime et al., 2023).

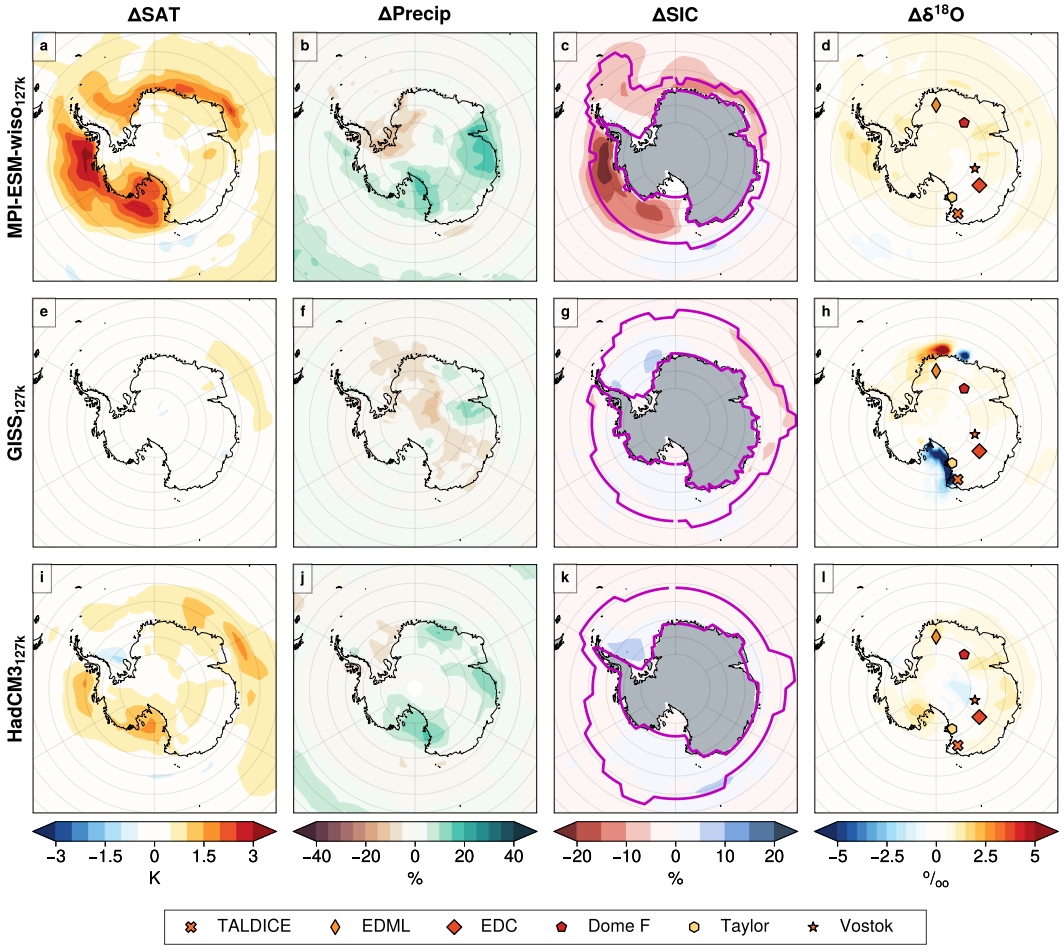

Figure 5. Anomalies in SAT, Precip, SIC and $\delta^{18}O$ over the Antarctic and Southern Ocean region for the 127k simulations compared to PI; all columns and rows as for Figure 1.

There are also variations across Greenland in ΔPrecip and $\Delta\delta^{18}O$ between the 127 k simulations. For example, $HadCM3_{127k}$ tends to be drier across southern Greenland, but the isotopic response over northern Greenland is much stronger, even when the precipitation increase there is weaker compared to MPI-ESM-wiso and GISS. This could be indicative of more detailed source and transport related response in $\delta^{18}O$. Although outside the scope of this manuscript, further water tracer-simulations might be useful to diagnose these (*e.g.* Gao et al., 2024b).

For the H11-200 and H11-3000 simulations $\Delta\delta^{18}O$ is depleted over Greenland and the wider northern Atlantic sector, commensurate with the mean-annual SIA increase and cooling (Section 3.1.2; and Figure 8). However, the warm Arctic and summer sea ice free Arctic of H11-overshoot leads to strongly enhanced precipitation and reduced sea ice, all of which contributes to

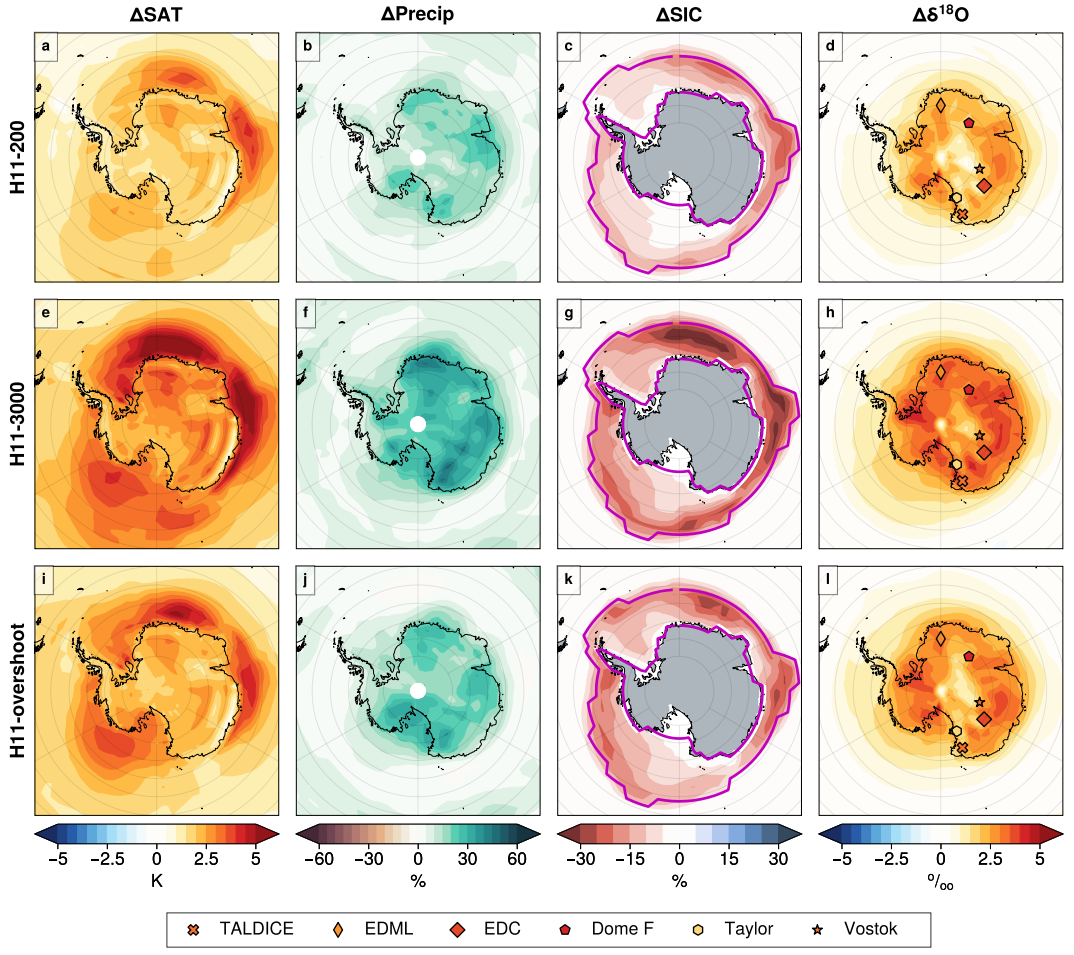

Figure 6. Anomalies in SAT, Precip, SIC and δ^{18}O over the Antarctic and Southern Ocean region for the H11 simulations; all columns and rows as for Figure 1. Note range of colorbars is wider than in Figure 5, except for δ^{18}O.

the very substantial H11-overshoot increase over Greenland core-mean $\Delta\delta^{18}$O of 2.8 ‰, compared to a Greenland core-mean $\Delta\delta^{18}$O of 3.2 ‰: *i.e.* H11-overshoot captures 81-87% of both summer Arctic ΔSAT and Greenland core-mean $\Delta\delta^{18}$O.

3.2.2 Antarctica

320 Section 3.1.3 indicated that the 127k simulations do not capture much of the observed Southern Ocean region warming. So in turn, the Antarctic ΔSAT, ΔPrecip, and $\Delta\delta^{18}$O 127k simulation changes are also very small, and not consistently in the correct direction relative to Antarctic core site 127ka measurements (Figure 5; Table A1): core-mean $\Delta\delta^{18}$O results are +0.0, -1.0, and +0.3 ‰ for HadCM3$_{127k}$, GISS$_{127k}$ and MPI-ESM-wiso$_{127k}$, respectively. This is compared with a observed core-mean $\Delta\delta^{18}$O

value of +3.3 ‰. This is somewhat like the Greenland 127k results; which also indicate that the mismatches with observed ice core $\Delta\delta^{18}O$ seem mostly driven by simulation of sea ice and SST changes, or lack thereof.

Within Antarctica, of the three 127k simulations, the MPI-ESM-wiso$_{127k}$ features the strongest Antarctic surface warming, including a strong warming around the west side of the Antarctic Peninsula and over other coastal regions. This likely is because it does show some 127k simulation Antarctic sea ice loss. The sea ice loss also leads to rather uniform $\delta^{18}O$ enrichment across the Antarctic and surrounding ocean. GISS$_{127k}$ and HadCM3$_{127k}$ show different patterns of $\Delta\delta^{18}O$ across Antarctica. HadCM3 simulates slight enrichment of $\delta^{18}O$ towards inland Antarctic, while GISS$_{127k}$ simulates strong enrichment around the Ross sea sector. Unlike MPI-ESM-wiso$_{127k}$, GISS$_{127k}$ and HadCM3$_{127k}$ do not show significant sea ice reduction, although HadCM3$_{127k}$ does simulate surface warming over Antarctic and coastal oceans, but not as strong as MPI-ESM-wiso$_{127k}$. GISS$_{127k}$ does not show any much change in ΔSAT. Both MPI-ESM-wiso$_{127k}$ and HadCM3$_{127k}$ have are wetter (larger ΔPrecip) over Ross sea sector. MPI-ESM-wiso$_{127k}$ is drier across Weddell sea to Dronning Maud Land, while GISS$_{127k}$ is drier inland, with only exception over East Antarctic from around 60-100 °E. It is difficult to know what, if anything, to draw from these multi-model variations.

Over Antarctica the H11 simulations show relatively uniform ΔSAT, ΔPrecip, and $\Delta\delta^{18}O$ (Figure 6). The H11 Antarctic core-mean values for: ΔSAT are +0.5K, +2.0, +3.0, and +2.4K at 0, 200, 3000 years and for the overshoot; and similarly of core-mean $\Delta\delta^{18}O$ values of +0.0, +1.9, 3.1, and +2.3 ‰ (Table A1; Figure 6), compared to the observed core-mean $\Delta\delta^{18}O$ value of 3.3 ‰. This means that H11-3000 simulation captures 94% of the observed Antarctic core-mean $\Delta\delta^{18}O$. This is commensurate with the previous sections which also show that the longer H11-3000 simulation also captures 50-100% of the Southern Ocean warming and sea ice loss.

3.3 The impact of changes in seasonality on $\Delta\delta^{18}O$

Decomposition of the impact of changes in seasonality on $\Delta\delta^{18}O$ can be useful to better understand drivers of $\Delta\delta^{18}O$. See Section 2.2.2 for a description of the breakdown of $\Delta\delta^{18}O$ into the two $\Delta Precip_{seasonal}$ (precipitation seasonality changes) and $\Delta\delta^{18}O_{seasonal}$ ($\delta^{18}O$ seasonality, or source effect, changes) that is used here.

3.3.1 Arctic

For the 127k simulations, precipitation source related ($\Delta\delta^{18}O_{seasonal}$) changes in the Arctic, particularly for MPI-ESM-wiso$_{127k}$ and GISS$_{127k}$ contribute strongly to the enrichment in $\delta^{18}O$ in regions of large sea ice loss; where there is increased exposure of the ocean surface there will be more (local) evaporation (Figure 7, first and third column). Given the large summer losses of Arctic sea ice, we would also expect to see an increase in summer precipitation for some simulations. Likely due their small Arctic SIAs, HadCM3$_{127k}$ and MPI-ESM-wiso$_{127k}$, do show the largest contribution from seasonal shift of precipitation (increase of warm season precipitation, $\Delta Precip_{seasonal}$), on $\Delta\delta^{18}O$ over Arctic. Indeed for HadCM3$_{127k}$ most increase in $\Delta\delta^{18}O$ is associated with these $\Delta Precip_{seasonal}$ precipitation seasonality changes. For MPI-ESM-wiso, the contributions of $\Delta Precip_{seasonal}$ and $\Delta\delta^{18}O_{seasonal}$ are more similar. Figure 1 and A3-A7 depict how $\Delta Precip_{seasonal}$ changes in these

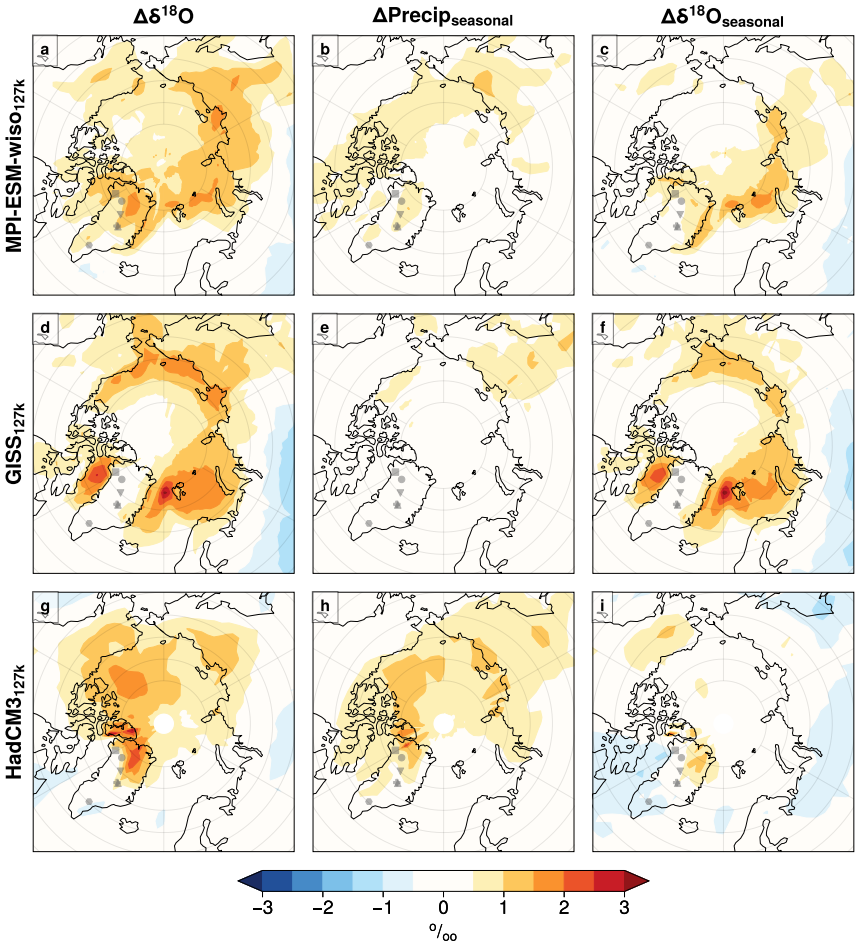

Figure 7. The impact of seasonality change on $\Delta\delta^{18}O$: decomposition of $\Delta\delta^{18}O$ values into contribution from seasonal variability into precipitation ($\Delta\mathtt{Precip}_{seasonal}$) and source variability ($\Delta\delta^{18}O_{seasonal}$) in the Arctic for the 127k simulations. See Section 2.2.2 for full details.

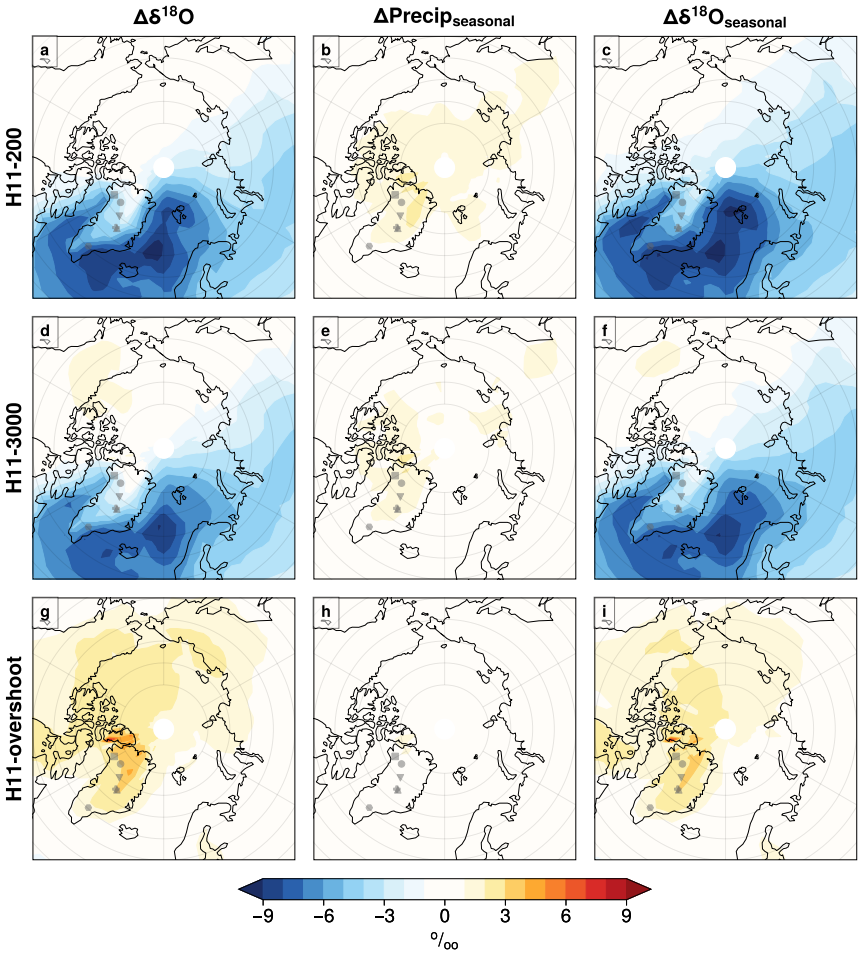

Figure 8. The impact of seasonality change on $\Delta\delta^{18}O$: : decomposition of $\Delta\delta^{18}O$ values into contribution from seasonal variability into precipitation ($\Delta\mathrm{Precip}_{seasonal}$) and source variability ($\Delta\delta^{18}O_{seasonal}$). Differences between the PI and H11 simulations, all columns and rows as for Figure 7.

models are depend largely on the loss of summertime high Arctic sea ice, which drives an increase in (local) warm season precipitation (Figure 7, middle column).

There is also some relationship between the two separate seasonality terms: the increased $\Delta\delta^{18}O_{seasonal}$ term does tend to contribute to the enrichment in $\delta^{18}O$ where ΔPrecip also increases (Figure 1), indicating that rainout and distance to source effects on $\delta^{18}O$ are sometimes closely related. As would be expected, where ΔPrecip decreases $\Delta\delta^{18}O_{seasonal}$ also tends to decrease.

For the H11 simulations, although $HadCM3_{127k}$ and H11-overshoot both show a warmer Arctic, the decomposition of $\Delta\delta^{18}O$ for each simulation shows distinctly different behaviour (Figure 10). As above, whilst for $HadCM3_{127k}$ most increase in $\Delta\delta^{18}O$ is associated with these $\Delta Precip_{seasonal}$, this is completely reversed for H11-overshoot, with almost all of the increase driven by $\Delta\delta^{18}O_{seasonal}$, rather than $\Delta Precip_{seasonal}$. This is because there is a large annual-mean, including wintertime, loss of sea ice in H11-overshoot, driven by the increased AMOC and global ocean temperature (rather than purely the orbital 127k spring-summer losses), leading to much more winter time, and closer sourced wintertime, precipitation over Greenland.

3.3.2 Antarctica

For the mainly orbitally-driven 127k simulations in Antarctica, precipitation seasonality changes ($\Delta Precip_{seasonal}$), contribute to depletion in $\delta^{18}O$ over Antarctica (Figure 9, middle column). For simulations where overall precipitation is increasing/not changing, including $HadCM3_{127k}$ and for the Ross Sea/East Antarctic sector in $MPI\text{-}ESM\text{-}wiso_{127k}$, this can be explained by relative increase in precipitation that falls during colder seasons during the 127k simulations relative to the PI, leading to reduced $\delta^{18}O$. However, opposing this, sea-ice retreat and shorter source-to-site vapour transport pathways can raise $\delta^{18}O$ values (Figure 9, right column). Together these two terms (the seasonality of precipitation, and seasonality of $\delta^{18}O$ changes) can therefore lead to rather small, sometimes near net near-zero simulated $\Delta\delta^{18}O$ across Antarctica between the LIG to PI for the 127k simulations (Figure 9).

The $GISS_{127k}$ simulation has a very unique pattern of $\delta^{18}O$ change in Antarctic with extreme low values over the Ross Sea sector and a very local pattern of low and high values in East Antarctic coastline around Dronning Maud Land. The surface temperature increase and sea ice reduction in Antarctic is minimal in this model compared to the other two, and the precipitation changes indicate change towards a drier 127k simulated Antarctic. We are unsure if the Antarctic $\delta^{18}O$ extremes indicate an issue with this particular simulation. We do not consider these extreme values further here.

The H11 simulations all show larger increases in $\delta^{18}O$ compared to the 127k simulations, in response to the increased SST/SAT and reduced sea ice. Here the negative precipitation seasonality changes, $\Delta Precip_{seasonal}$, are dwarfed by the impact of the $\Delta\delta^{18}O_{seasonal}$ terms. This means that sea-ice retreat and shorter source-to-site vapour transport pathways, particularly in the colder and shoulder seasons act to strongly raise $\delta^{18}O$ values (Figure 10, right column). For H11-overshoot, the Antarctic and Southern Ocean temperature and sea ice does not reverse to its pre-H11 state (*i.e.* $HadCM3_{127k}$ state) after 200 years of no meltwater: once the AMOC recovered to the initial strength (Figure A2) elevated global and polar temperature take time to cool, thus Antarctic $\delta^{18}O$ values remain high more than 200 years after the H11-hosing has stopped.

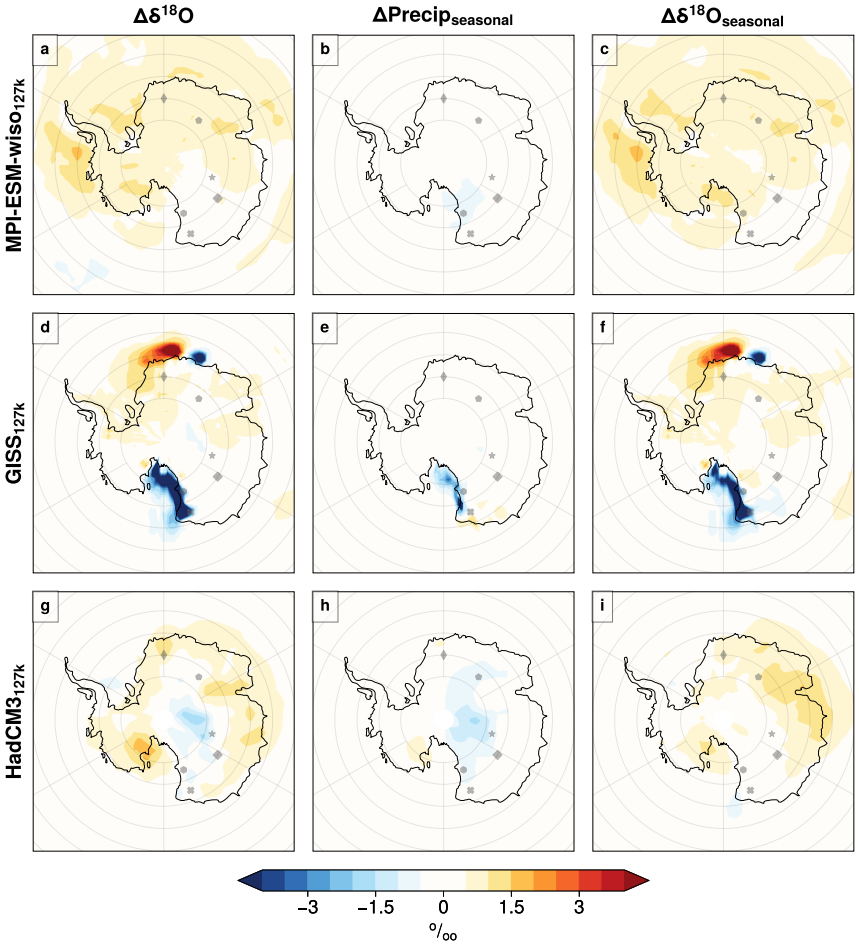

Figure 9. The impact of seasonality change on $\Delta\delta^{18}O$: decomposition of $\Delta\delta^{18}O$ values into contribution from seasonal variability into precipitation ($\Delta\mathrm{Precip}_{seasonal}$) and source variability ($\Delta\delta^{18}O_{seasonal}$). Differences between the PI and 127k simulations for the Antarctic region, all columns and rows as for Figure 7.

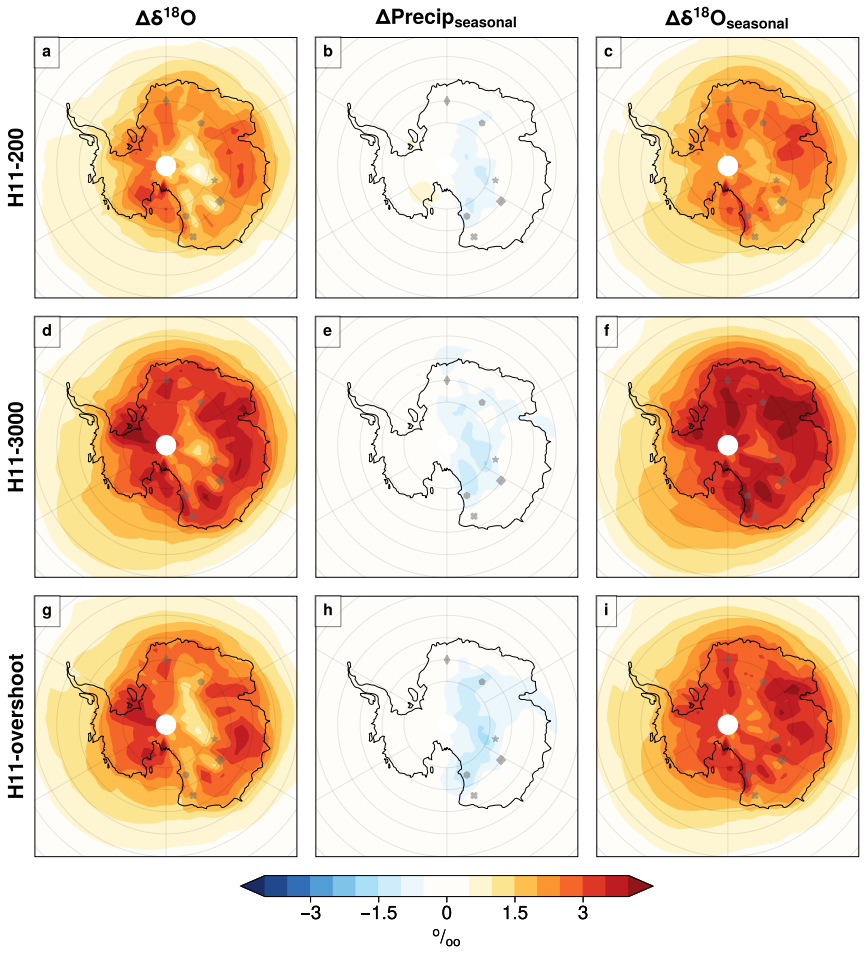

Figure 10. The impact of seasonality change on $\Delta\delta^{18}O$: decomposition of $\Delta\delta^{18}O$ values into contribution from seasonal variability into precipitation ($\Delta Precip_{seasonal}$) and source variability ($\Delta\delta^{18}O_{seasonal}$). Differences between the PI and H11 simulations for the Antarctic region, all columns and rows as for Figure 7.

Table 2. Relationships between SAT and $\delta^{18}O$, calculated using all model simulations for each site. Fits use $\Delta\delta^{18}O$ as the dependant variable and ΔSAT as the independent variable, to enable projection of ΔSAT from $\Delta\delta^{18}O$. See also Section 2.2.3. The projected ΔSAT values are shown with 95% confidence intervals, and are based on the ice core $\Delta\delta^{18}O$ values in Table A1.

Site	Slope	STDERR	Projected SAT
	K per ‰	K per ‰	K
	Arctic core sites		
NEEM	0.8	0.1	2.89 ± 1.32
NGRIP	1.08	0.14	3.36 ± 1.92
GRIP	1.09	0.17	3.49 ± 2.5
GISP2	1.09	0.14	2.94 ± 2.04
Camp_century	0.73	0.14	1.46 ± 1.78
DYE3	0.56	0.09	2.62 ± 2.45
	Antarctic core sites		
Vostok	1.04	0.19	3.44 ± 2.42
Dome F	0.97	0.05	4.35 ± 0.75
EDC	1.1	0.1	4.39 ± 1.45
EDML	0.91	0.1	2.65 ± 1.54
TALDICE	0.52	0.2	1.67 ± 3.67
Taylor	0.62	0.2	1.18 ± 2.67

Overall, for Antarctica every $\Delta Precip_{seasonal}$ result for the six simulation is small, with some negative regions (more colder season precipitation). $\Delta\delta^{18}O_{seasonal}$ is always larger and tends to dominate Antarctic $\Delta\delta^{18}O$ for each simulation, mostly due to sea ice related changes (Figures 5, 9, and 10, first and last columns).

3.4 Implications for the interpretation of ΔSAT from $\Delta\delta^{18}O$ in ice cores

The interpretation of $\Delta\delta^{18}O$ values in polar ice cores as a proxy for past temperatures is a critical component of paleoclimate reconstructions. Past LIG temperature estimates derived from $\delta^{18}O$ values at key Greenland and Antarctic sites, such as NEEM, Dome C, Vostok, and Dome F, have generally been obtained by converting $\Delta\delta^{18}O$ to SAT using palaeothermometer gradients. For instance in Greenland at the NEEM ice core, NEEM community members (2013) converted $\Delta\delta^{18}O$ to SAT using a palaeothermometer gradient of 2.1 ± 0.5 K/‰, which was based on data from Vinther et al. (2009). This means that the NEEM $\Delta\delta^{18}O$ value of $+3.6$ ‰ implies that, without taking account of any ice flow influences on site temperature, peak LIG surface temperatures were $+7.5 \pm 1.8$ K warmer than the PI.

For Antarctica, Jouzel et al. (2007) applied a gradient of 1.43 K/‰, Petit et al. (1999) and Masson-Delmotte et al. (2006) used a gradient of 1.33 K/‰, whilst Sime et al. (2009), based on isotope-enabled model simulations focussed on 2100, proposed a palaeothermometer gradient for the East Antarctic Dome C (EDC) core around 1.7 K/‰, and suggested that regional and

temporal variability in the paleothermometer gradient might be more significant than previously thought. The simulations presented here enable examination of the consistency of the relationships between ΔSAT and $\Delta\delta^{18}O$ across all the LIG_{127k} and LIG_{H11} simulations.

Standard errors and uncertainties for gradients for H11 simulations are smaller then where LIG_{127k} simulation results are used alone (Tables 2 and A5). This is primarily because the H11 simulations show larger ΔSAT and $\Delta\delta^{18}O$ values than the 127k simulations, so exert a stronger influence on the gradient of the regression lines fitted to ΔSAT and $\Delta\delta^{18}O$ (Figure 11 and Table A1). Given Sections 3.1-3.3 show that these H11 simulations do a better job of capturing peak LIG warmth and sea ice changes at both poles, compared to the 127k simulations, this larger influence seems reasonable. We also find that if regression fits are applied to LIG_{127k} simulation results alone, without including the H11 simulations, gradients are not inconsistent, if very uncertain (Table A5). This suggests that the underlying physics driving the $\delta^{18}O$-SAT relationship is consistent across different LIG climate states, even if the 127k simulations alone are insufficient to derive accurate gradients. Here we therefore use the all simulation results to derive LIG temperature estimates from $\Delta\delta^{18}O$ values at Greenland and at Antarctic core sites.

The results in this section use primarily one-part fits (Section 2.2.3). These assume that ΔSAT and $\Delta\delta^{18}O$ are co-dependent; that they always tend to change together. However note that using a two-part fit *i.e* a regression line which permits a non-zero intercept (Table A7 and Figure A9) give results which are agree, within uncertainties, with these one-part fits. Thus this choice is not significant to our findings. Section 2.2.3 explains fit methods, and the calculation of uncertainties.

3.4.1 Greenland - NEEM

The interpretation of LIG temperature from $\Delta\delta^{18}O$ values measured in Greenland ice has only been attempted for the NEEM ice core (NEEM community members, 2013). This is likely because, as outlined in Section 2.3, the dating of LIG ice for most Greenland ice cores is difficult due to stratigraphic disturbances in the ice of this age. Interestingly, the simulations used here show a substantially lower gradient of 0.8 K/‰ at NEEM, less than half of that used in NEEM community members (2013). Other ice core sites in central Greenland have a slightly higher gradient of around 1.1 K/‰ at NGRIP, GRIP, and GISP2. Based on the Section 2.3 value (in Table A1), these suggest that, without taking account of any site elevation or other ice flow effects, there was a PI to LIG warming of $+2.89 \pm 1.32$ K at NEEM, and $+3.49 \pm 2.5$ K at GRIP. Table 2 and Figures 11 and 12a show that the gradients across Greenland are relatively uniform, but with a tendency towards higher K/‰ gradients inland compared to the coast.

3.4.2 Antarctica

The relationship between $\Delta\delta^{18}O$ and ΔSAT shows considerable variation across Antarctica (Figure 12, Antarctic row), particularly between the high EAIS Plateau (like Vostok, Dome F and EDC) and more coastal sites (like Taldice and Taylor): gradients tend to be higher across the Plateau (Table 2). This same spatial pattern in gradients is also reflected in relationships between $\Delta\delta^{18}O$ and other quantities like ΔSIA (Figure A8). These differences underscore that it may be necessary to use site and time-specific paleothermometer gradients rather than applying a uniform and constant gradient across all Antarctic locations and periods. Like Greenland above, central Antarctica has higher K/‰ gradients compared to the coastal regions.

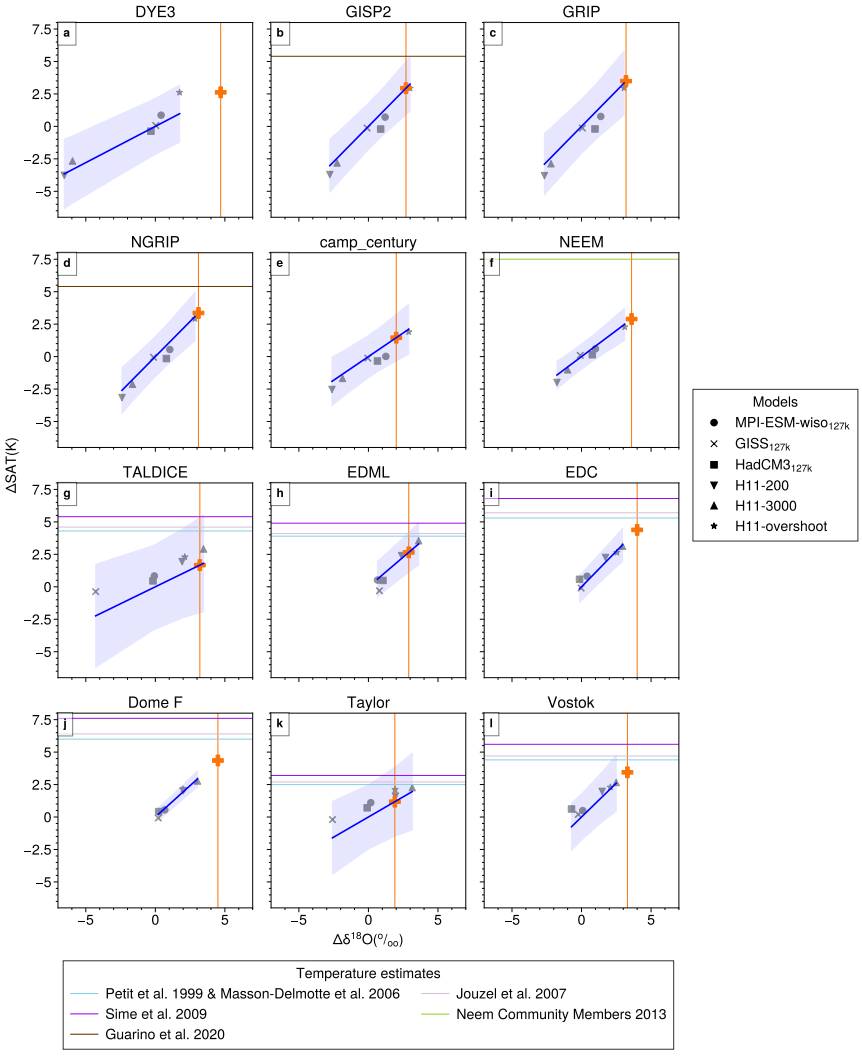

Figure 11. $\Delta\delta^{18}O$ versus ΔSAT for different simulations, for each ice core site. Fits are calculated as described in Section 2.2.3. Shaded bands show the 95% uncertainty envelope. Vertical orange line indicate the ice core $\Delta\delta^{18}O$ values (Table A1). Horizontal lines indicates temperature estimates for each ice core location from previous studies, whilst orange crosses indicates our estimated central ΔSAT values obtained from the simulation fits *i.e.* projected using the fitted modelled $\Delta\delta^{18}O$ - ΔSAT (blue line) relationships.

The gradients derived from these simulations at the Vostok, Dome F, and EDC ice core sites range from 0.9 K/‰ to 1.1 K/‰. These are a little lower than the canonical values often used in previous studies ($1.3-1.4\,\mathrm{K}/‰$) (Petit et al., 1999; Masson-Delmotte et al., 2006; Buizert et al., 2021). For example, Werner et al. (2018) set up eight atmospheric model simulations using ECHAM5-wiso with different Last Glacial Maximum (LGM) ice sheet reconstructions to investigate the temporal and spatial relationships between δ^{18}O and SAT across Antarctica. They found that, whilst these LGM to PI relationships differed across Antarctic regions, they tended to be close to a commonly identified relationship of around $1.25\,\mathrm{K}/‰$. That said, Cauquoin et al. (2023) note that ECHAM5-wiso tends to significantly overestimate isotope changes in Antarctica compared to more recent ECHAM6-wiso simulations, even under identical boundary conditions. Thus some questions do remain LGM to PI $\Delta\delta^{18}$O and ΔSAT relationships. Indeed it is possible, as yet, we do not have reliable multi-model isotopically enabled LGM simulations.

Applying these LIG multi-model simulation-derived gradients to the $\Delta\delta^{18}$O ice core values in Table A1 yields inferred past peak interglacial surface air temperature increases. These are: 4.35 ± 0.75 K for Dome F, 3.44 ± 2.42 K for Vostok, and 4.39 ± 1.45 K for EDC, on the High EAIS Plateau. For the more coastal sites of TALDICE and Taylor, more modest increases of 1.67 ± 3.67, and 1.18 ± 2.67 are inferred. However, if two-part fits are allowed for these coast sites *i.e* SAT can rise between PI and peak-LIG, Table A7 show larger past peak interglacial surface air temperature increases of: 2.52 ± 1.36, and 1.78 ± 0.66, which are somewhat closer to the inland core site rises.

In summary, these results together suggest a more modest PI to peak-LIG temperature increase across Antarctica compared to earlier estimates. We attribute this difference primarily to the substantially improved representation of LIG sea surface conditions around Antarctica, particularly for sea ice, which enables a better representation of the key ΔSAT, ΔPrecip, and $\Delta\delta^{18}$O changes.

4 Conclusions

The Last Interglacial (LIG), from about 130,000 to 115,000 years ago, is one of the warmest periods in recent geological history (Hoffman et al., 2017; Fischer et al., 2018), with warming that may be similar to predictions for the end of this century (IPCC, 2021). However, reconstructing peak LIG temperatures around 127 ka from ice cores can be challenging due to unknowns about the relationship between water isotopes (δ^{18}O) and temperature.

This study used three isotope-enabled climate models—HadCM3, MPI-ESM-wiso, and GISS ModelE-R—in the first multi-model analysis of the LIG. Standard 127k simulations, following the PMIP4 (orbital and greenhouse gases) protocol (Otto-Bliesner et al., 2017), were run for each model. These simulations were complemented with a long 3000-year LIG H11 simulation run using HadCM3.

The 127k simulations tend to show slight global cooling, but the H11 simulations, especially the extended H11-3000 and H11-overshoot simulations, capture significant warming trends that are consistent with the LIG observations of peak warmth (Fischer et al., 2018; Shackleton et al., 2020). In particular, the H11-overshoot simulation appears to accurately represent peak LIG Arctic conditions, replicating 81% of the peak summer temperature increase, reducing summer sea ice by 75%, and

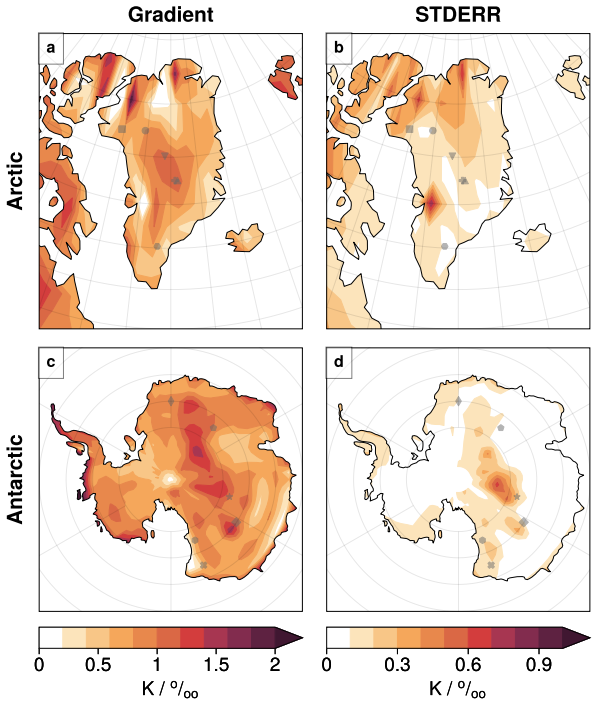

Figure 12. Maps of $\Delta\delta^{18}O$ versus ΔSAT gradient and associated standard error, calculated at each grid point using all simulations. Fitting procedure described in Section 2.2.3, and show for example ice core sites in Fig. 11.

showing periods of nearly ice-free Arctic summers. This simulation also matched the observed peak LIG changes in Greenland ice core $\delta^{18}O$, with a 2.8 ‰ increase, close to the observed 3.2 ‰. We note that some parts of the remaining 0.4‰ missing part of the simulated isotope signal could be due to vegetation or ice sheet feedbacks which are not included in these simulations (Claussen et al., 2006; Schurgers et al., 2007; Nikolova et al., 2013; Otto-Bliesner et al., 2006). Further, we note that the lack of an sea ice-free Arctic in summer in the 127k simulations may reflect deficiences in the sea ice submodel (Guarino et al., 2020; Diamond et al., 2023; Sime et al., 2023). In future, Arctic and Greenland $\delta^{18}O$ results in models with alternative sea ice submodels should be explored.

In Antarctica, the H11-3000 simulation successfully captured 50-100% of the peak LIG Southern Ocean warming and sea ice loss and 94% of the observed increases in ice core $\Delta\delta^{18}O$. This highlights both the importance of including prolonged meltwater events in climate models to accurately capture peak LIG conditions, and the necessity of a good polar climate to simulate ΔSAT, ΔPrecip, and $\Delta\delta^{18}O$ over the ice sheets.

Our H11 simulation is highly idealised (Holloway et al., 2018; Gao et al., 2024a), and so we emphasise it cannot be tied to particular time points within the LIG. On timing however, Shackleton et al. (2020)'s recent results suggest a LIG peak in GMOT around 129ka. Our simulation results suggest this should be co-incident with the end of the H11 - NH deglaciation - meltwater event. This appears to in agreement with Stoll et al. (2022), who show that whilst the bulk of the Northern Hemisphere

deglacial occurred between 134-130ka, global sea level continued to increase due to meltwater until 129ka or a little after. Additionally, given H11-3000 simulates our warmest Southern Ocean and Antarctic state, and within a hundred years H11-overshoot simulates our warmest Arctic and Greenland state, peak SST and SAT temperatures, and a minimum in SIA, may have occurred within a rather short time-span for both Greenland and Antarctica. Time-scales for deeper ocean changes are however slower, and will have a different pattern of evolution. Further work should examine how short-lived the H11-overshoot is for the Arctic, alongside its interaction with the period of very-high early-summer insolation that is also centred around 127ka.

The use of $\Delta\delta^{18}O$ values in polar ice cores as a temperature proxy is key to reconstructing past climates. Temperature estimates from $\delta^{18}O$ at sites like NEEM, Dome C, Vostok, and Dome F during the Last Interglacial (LIG) rely on converting $\Delta\delta^{18}O$ into ΔSAT using palaeothermometer gradients. Our simulations suggest a gradient of 0.8 K/‰ at NEEM, which is less than half that used by NEEM community members (2013), with slightly higher values, around 1.1 K/‰, at central Greenland sites such as NGRIP, GRIP, and GISP2. Interestingly, these revised values are quite close to those from Lee et al. (2008), who find spatial relationships of about 0.8 K/‰ between annual mean temperature at the top of the inversion layer and annual mean $\delta^{18}O$ in precipitation (Liu et al., 2023). Further work is needed to understand the role of inversion layers in shaping these relationships during the LIG. In future studies, it may also be valuable to examine local-to-regional influences, such as changes in local boundary layer conditions (Krinner et al., 1997; Noone and Simmonds, 2002) and continental vapor recycling impacts (Werner et al., 2001; Werner and Heimann, 2002; Sjolte et al., 2014), alongside larger-scale effects such as distal source property and pathway changes (Boyle, 1997; Kindler et al., 2014; Guan et al., 2016). Isotope-enabled models, and associated water tracking tools, are particularly helpful for ensuring that these factors are included when examining relationships between $\Delta\delta^{18}O$ and ΔSAT (Jouzel et al., 1997; Gao et al., 2024b; McLaren et al., 2025).

Use of these $\Delta\delta^{18}O$–ΔSAT relationships from the new LIG simulations suggests PI-to-LIG warming values of $+2.89 \pm 1.32$ K at NEEM and $+3.49 \pm 2.5$ K at GRIP. These estimates do not account for site elevation or ice flow effects and are substantially lower than previously suggested warming values. For Antarctica, our simulated $\delta^{18}O$–temperature gradients at sites including Dome C, Dome F, and Vostok range from 0.9 K/‰ to 1.1 K/‰, slightly lower than previously published values of 1.3–1.4 K/‰ (Petit et al., 1999; Masson-Delmotte et al., 2006). Applying these updated gradients, the estimated peak temperature increases between the PI and LIG are 4.39 ± 1.45 K for Dome C, 4.35 ± 0.75 K for Dome F, and 3.44 ± 2.42 K for Vostok. These findings suggest a more modest temperature rise during the LIG for both Greenland and Antarctica than previously thought. This revision is largely due to improved representation of polar sea ice changes in the new extended H11 simulations.

However, it is important to note that these revised temperature estimates do not incorporate any corrections for ice core site elevation or other ice flow-related impacts on site temperatures. Future efforts should focus on better characterizing LIG Antarctic and Greenland ice sheet changes, which influence both $\delta^{18}O$ and temperature (Holloway et al., 2016; Werner et al., 2018; Domingo et al., 2020; Goursaud et al., 2021; Zou et al., 2025), as well as on the role of potential vegetation feedbacks (Claussen et al., 2006; Schurgers et al., 2007; Nikolova et al., 2013; Otto-Bliesner et al., 2006). In addition, a re-examination of the nature and timing of peak polar ice sheet warmth, and its co-incidence between Antarctica and Greenland, is warranted.

Finally, the application of newly developed water tracking tools in climate models may provide further insight into the drivers of $\Delta\delta^{18}O$–ΔSAT relationships (Gao et al., 2024b; McLaren et al., 2025), alongside the use of more advanced sea ice submodels (Diamond et al., 2023; Sime et al., 2023).

Code availability. All code used to produce the figures and tables is available on zenodo: https://doi.org/10.5281/zenodo.14640495.

Data availability. The model datasets used to produce the figures and tables are available on zenodo: https://doi.org/10.5281/zenodo.14640495. Last Interglacial summer air temperature observations for the Arctic (Version 1.0) are also published by the NERC EDS UK Polar Data Centre here: https://doi.org/10.5285/9AB58D27-596A-472C-A13E-2DCD68612082. The Capron et al. (2017) and Hoffman et al. (2017) datasets are available from: https://doi.org/10.1016/j. quascirev.2017.04.019. The Chandler and Langebroek (2021a) dataset is available from: https://doi.org/10.1594/PANGAEA.938620. The Chadwick et al. (2021) dataset is available from: https://doi.org/10.1594/PANGAEA.936573. The four paleoclimate syntheses by Gao et al. (2024) from: https://zenodo.org/records/11079974. The Greenland ice core data is available in Table 1 of: https://doi.org/10.1029/2019JF005237. The Antarctic ice core data is available in Table S3 of: https://doi.org/10.1029/2020GL091412.

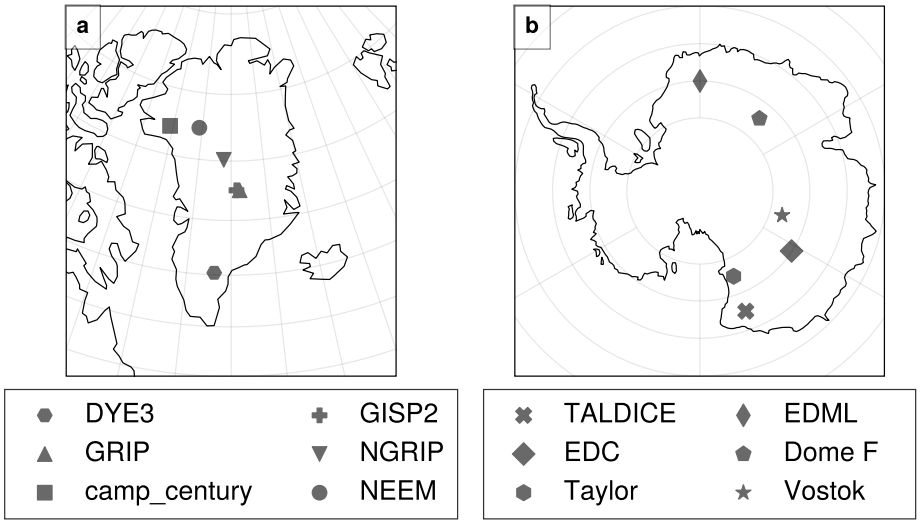

Figure A1. The locations of the Greenland and Antarctic ice core sites.

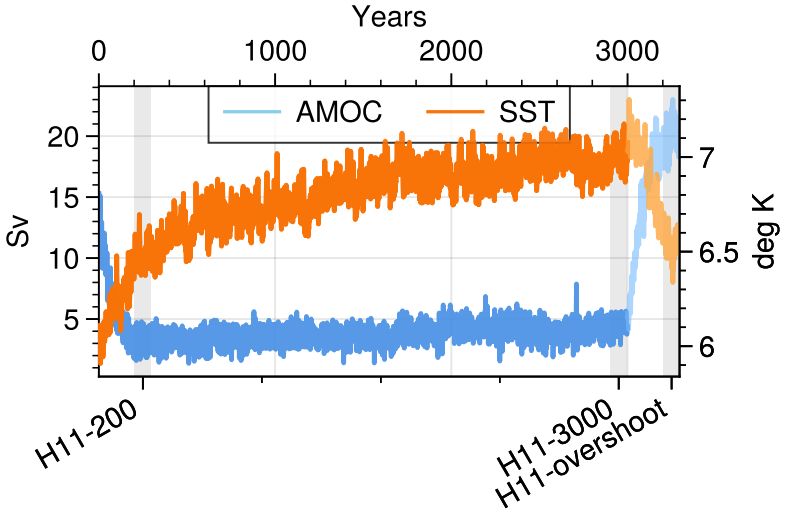

Figure A2. Time series of AMOC (in Sv) and average Southern Hemisphere SST (south of 40°S) time series from HadCM3 H11 simulations. The lighter colors represent the period where the water hosing was stopped. The three grey bands denote the three selected slices from this simulation: H11-200; H11-3000; and H11-overshoot.

Appendix A

A1

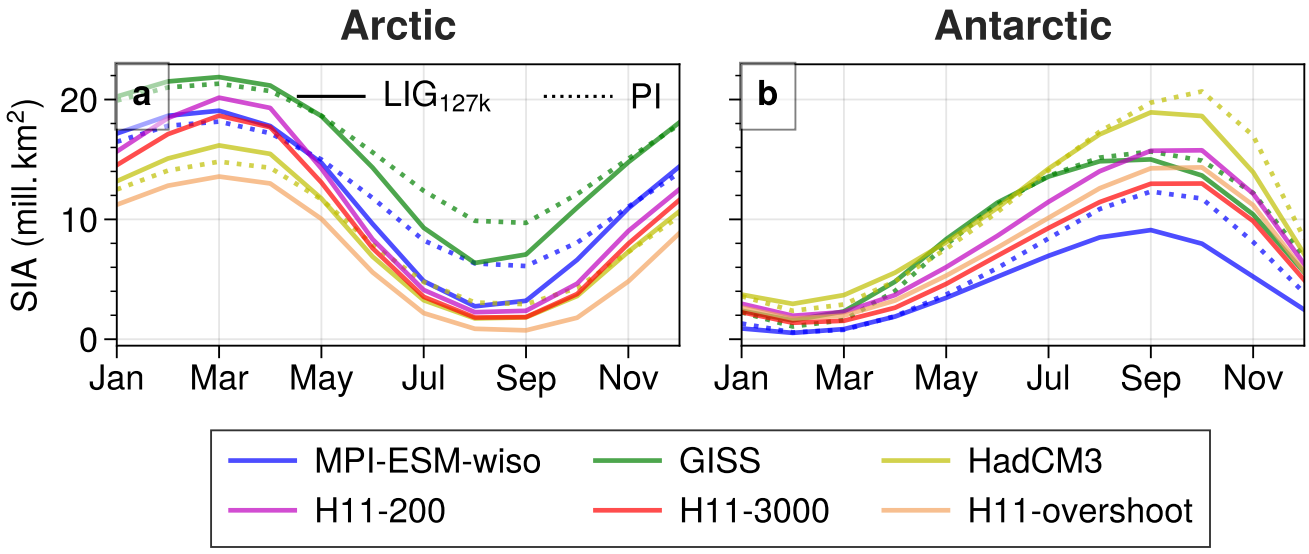

Figure A3. Seasonal cycle of total sea ice area in the Northern and Southern Hemisphere, for each simulation. These are absolute values (not Δ values). LIG values are shown using solid lines and PI values are the dotted lines.

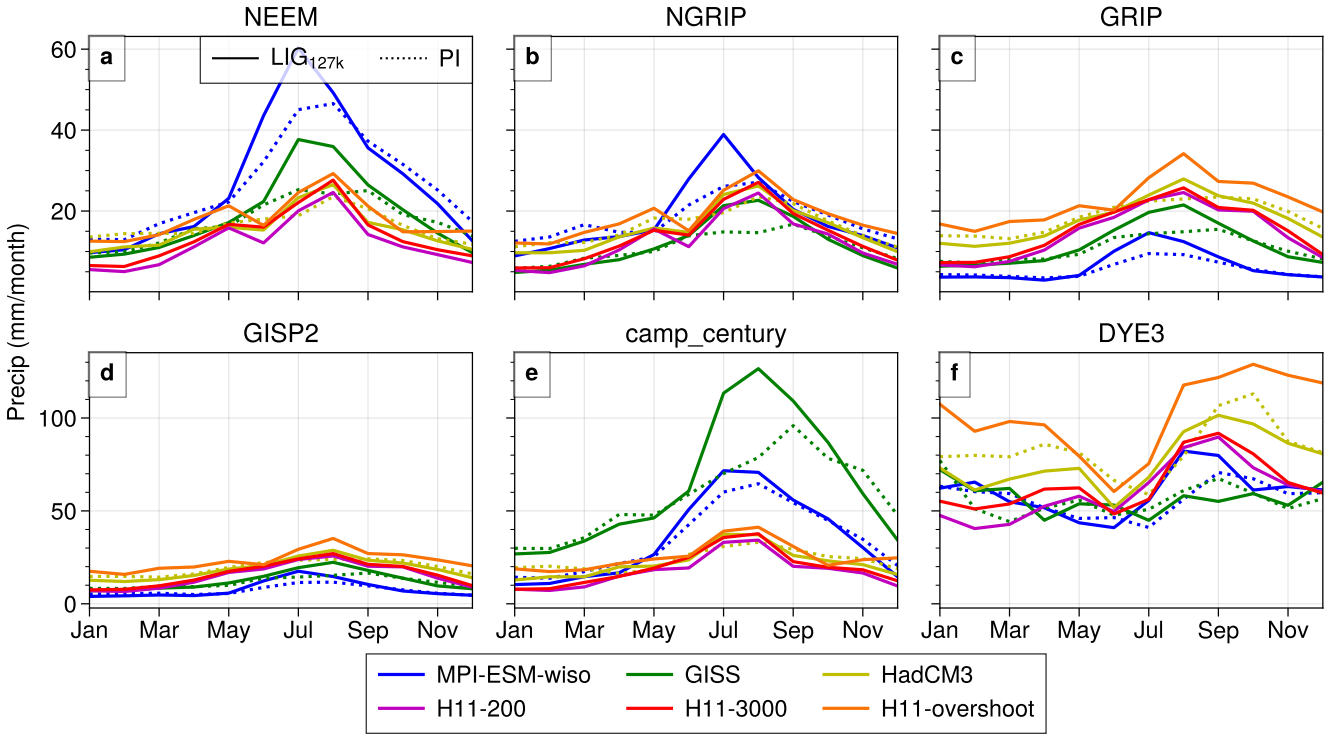

Figure A4. Seasonal cycle of precipitation at each ice core site in Greenland. These are absolute values (not Δ values). LIG values are shown using solid lines and PI values are the dotted lines.

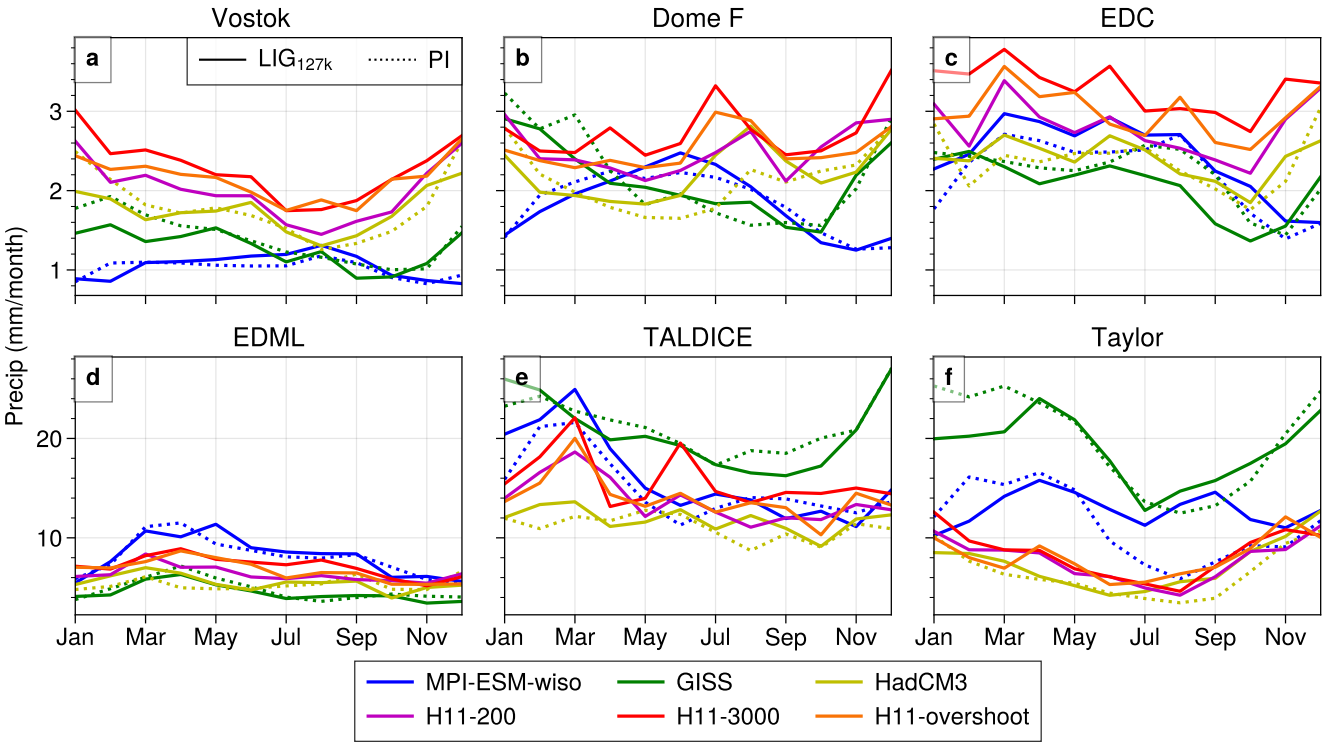

Figure A5. The seasonal cycle of precipitation, as Figure A4, but for Antarctica.

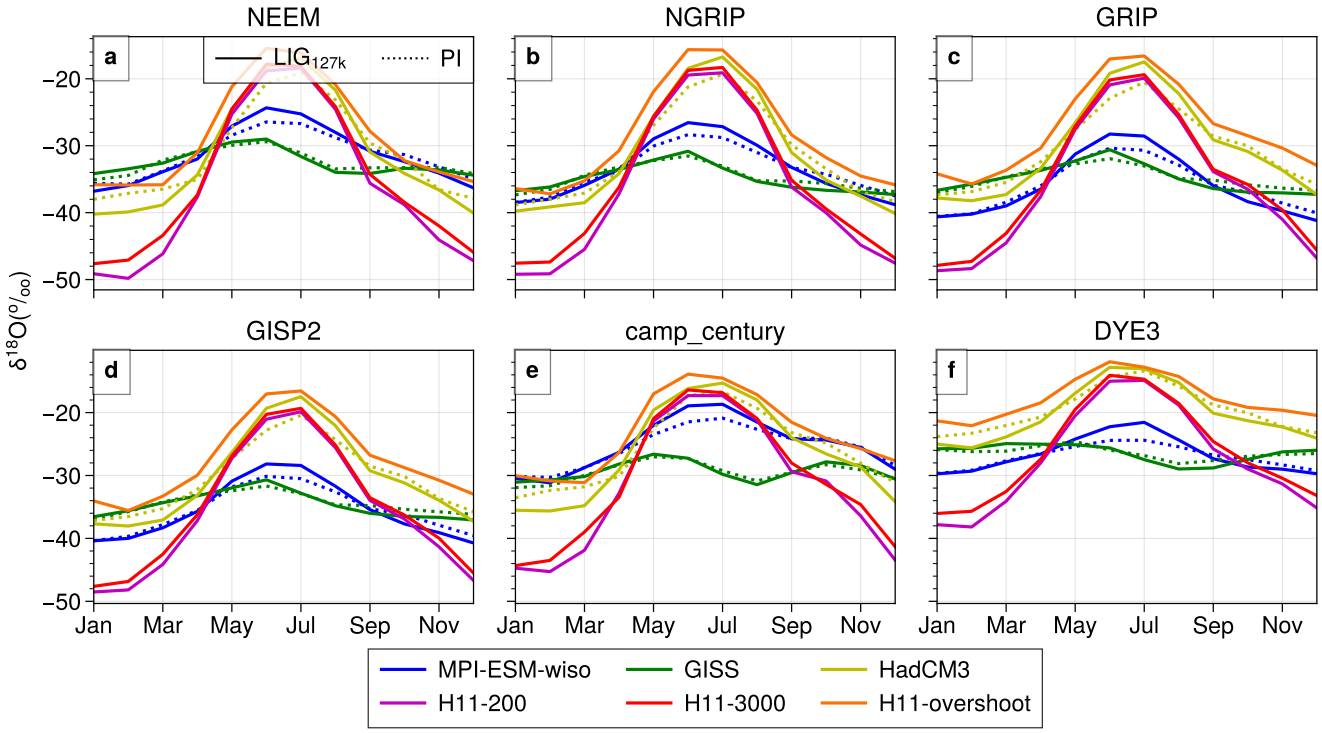

Figure A6. The seasonal cycle of $\delta^{18}O$, otherwise as Figure A4.

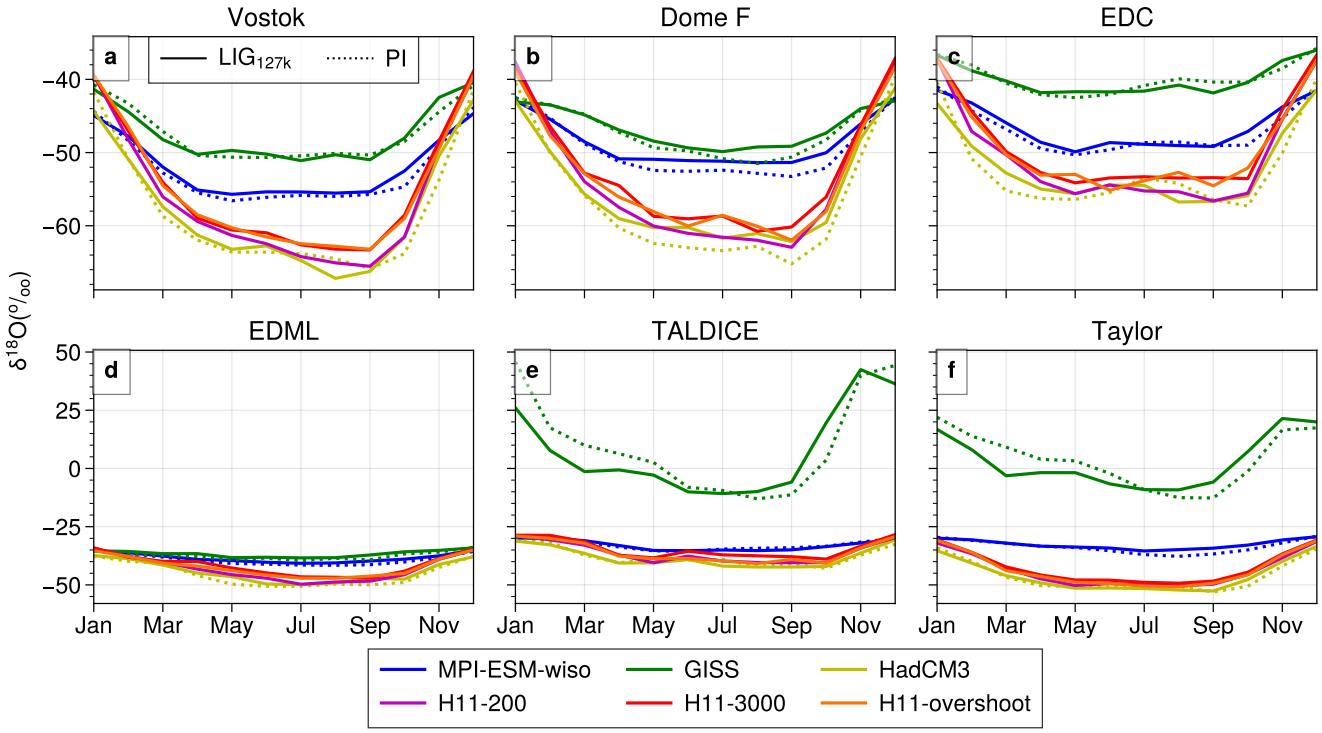

Figure A7. The seasonal cycle of $\delta^{18}O$ for Antarctica, otherwise as Figure A6.

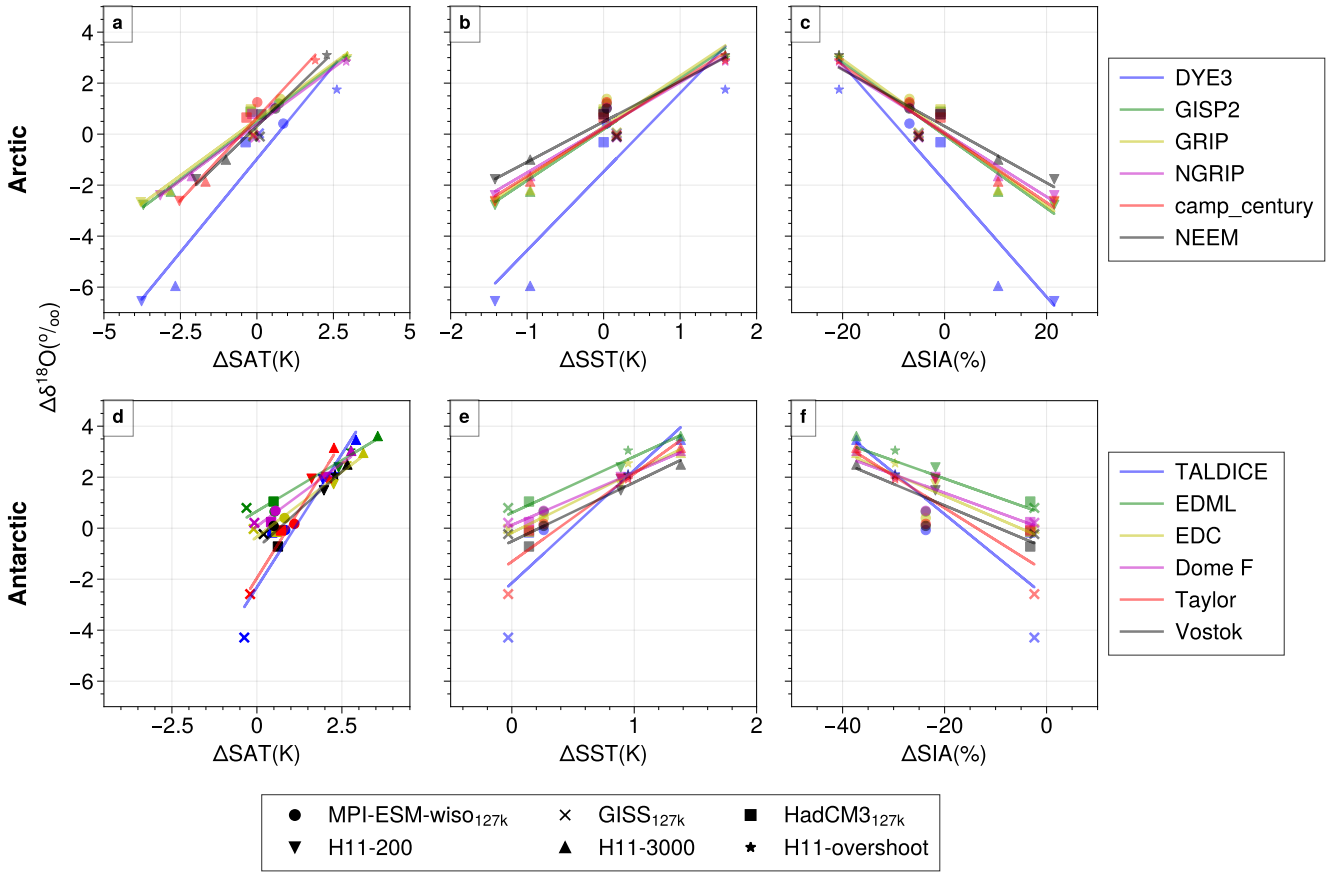

Figure A8. ΔSAT at each ice core location (first column), Δ SST (north/south of 40°latitude for Arctic and the Antarctica) and ΔSIA (annual sea ice area) versus $\Delta\delta^{18}O$ from each ice core sites, for all simulations.

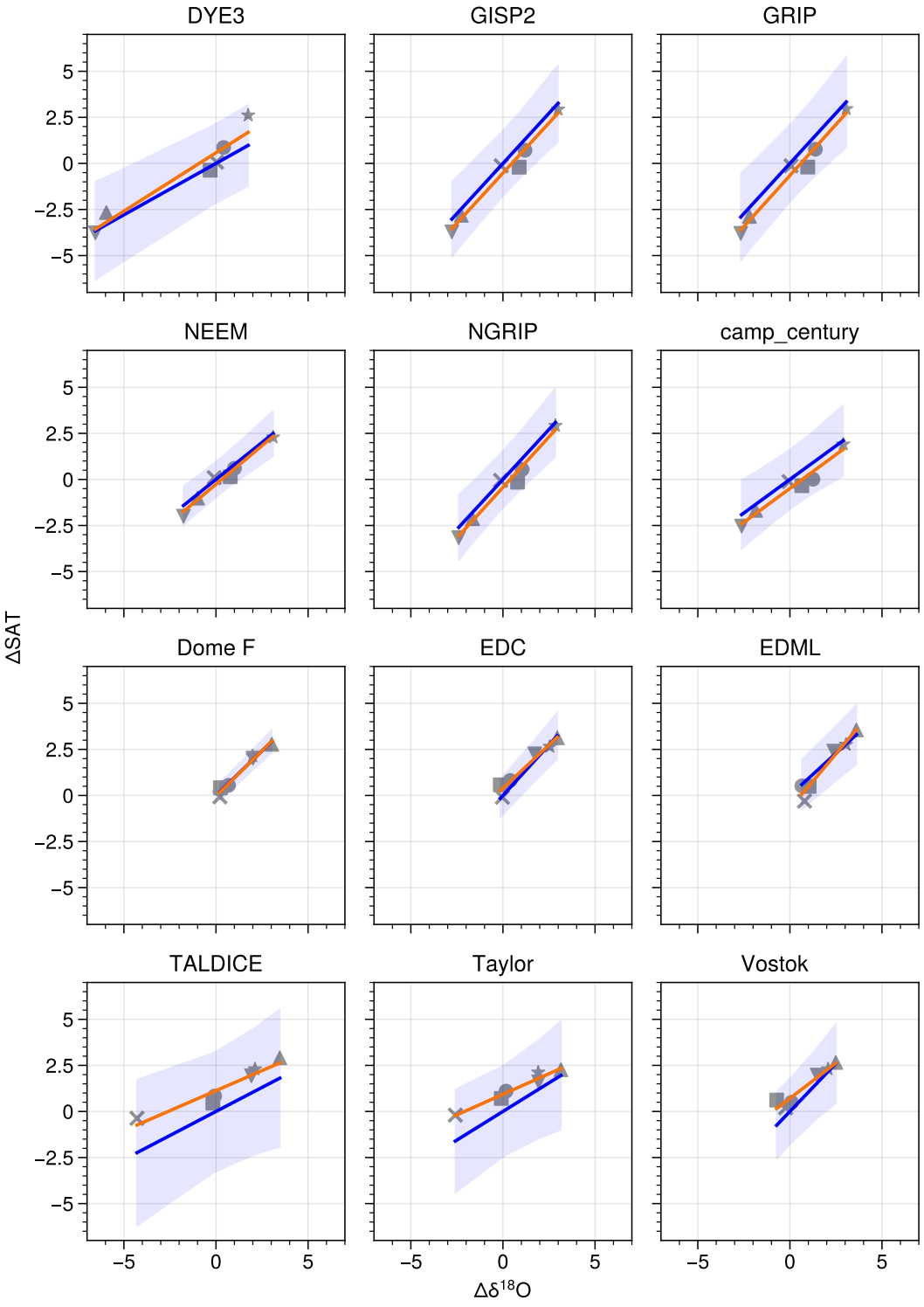

Figure A9. Same as 11, but using a two-part fit *i.e* a regression line which permits a non-zero intercept (orange lines).

Table A1. Ice core and simulated $\Delta\delta^{18}O$ values at ice core locations, and simulated ΔSAT.

			Ice Core	MPI-ESM-wiso$_{127k}$		GISS$_{127k}$		HadCM3$_{127k}$		H11-200		H11-3000		H11-overshoot	
SITE	LON	LAT	$\Delta\delta^{18}O$	ΔSAT	$\Delta\delta^{18}O$	ΔSAT	$\Delta\delta^{18}O$	ΔSAT	$\Delta\delta^{18}O$	ΔSAT	$\Delta\delta^{18}O$	ΔSAT	$\Delta\delta^{18}O$	ΔSAT	$\Delta\delta^{18}O$
Greenland Core Sites															
NEEM	-51.1	77.4	3.6	0.6	1.0	0.1	-0.1	0.1	0.8	-2.0	-1.8	-1.3	-1.0	2.3	3.1
NGRIP	-42.3	75.1	3.1	0.5	1.0	-0.0	-0.1	-0.2	0.8	-3.2	-2.4	-2.3	-1.6	2.9	2.8
GRIP	-37.6	72.6	3.2	0.8	1.4	-0.1	0.1	-0.2	1.0	-3.8	-2.7	-3.0	-2.2	3.0	3.1
GISP2	-38.5	72.6	2.7	0.7	1.2	-0.1	-0.1	-0.2	0.9	-3.7	-2.8	-2.9	-2.3	2.9	3.0
Camp Century	-61.1	77.2	2.0	0.0	1.3	-0.1	-0.0	-0.3	0.6	-2.5	-2.6	-2.0	-1.9	1.9	2.9
DYE3	-43.8	65.2	4.7	0.9	0.4	0.1	0.0	-0.4	-0.3	-3.8	-6.6	-2.9	-6.0	2.6	1.7
Mean	-	-	3.22	0.6	1.0	-0.0	-0.0	-0.2	0.6	-3.2	-3.1	-2.4	-2.5	2.6	2.8
Antarctic Core Sites															
Vostok	106.5	-78.3	3.3	0.5	0.1	0.2	-0.2	0.6	-0.7	2.0	1.5	2.7	2.5	2.3	2.1
Dome F	39.4	-77.2	4.5	0.6	0.7	-0.1	0.2	0.4	0.2	2.0	2.0	3.0	3.0	2.1	2.0
EDC	123.2	-75.1	4.0	0.8	0.4	-0.1	-0.0	0.6	-0.1	2.3	1.7	3.4	3.0	2.6	2.5
EDML	0.0	-75.0	2.9	0.5	0.6	-0.3	0.8	0.5	1.0	2.4	2.4	3.7	3.6	2.8	3.0
TALDICE	159.1	-72.5	3.2	0.8	-0.1	-0.4	-4.3	0.4	-0.2	1.9	1.9	3.0	3.5	2.3	2.1
Taylor	158.4	-77.5	1.9	1.1	0.2	-0.2	-2.6	0.7	-0.1	1.6	1.9	2.3	3.2	2.1	1.9
Mean	-	-	3.3	0.7	0.3	-0.1	-1.0	0.5	0.0	2.0	1.9	3.0	3.1	2.4	2.3

Table A2. Global mean ΔSAT , Δ SST, and Δ GMOT (Global Mean Ocean Temperature) for each simulation.

Experiment	ΔSST	ΔSAT	ΔGMOT
MPI-ESM-wiso$_{127k}$	-0.07	-0.11	-0.045
GISS$_{127k}$	-0.17	-0.15	-
HadCM3$_{127k}$	-0.14	-0.23	-0.016
H11-200	0.04	-0.23	-
H11-3000	0.45	0.35	0.84
H11-overshoot	0.83	1.09	0.78

Table A3. Simulated Arctic and Antarctic ΔSAT and ΔSIA values. Column 1: mean Δ SAT (averaged north of 60°N for Arctic and south of 60°S for Antarctic). Column 2: annual LIG sea ice area (mill. km^2). Column 3: LIG-PI anomaly in SIA (in %). Column 4: summer mean Δ SAT (JJA averaged north of 60°N for Arctic and DJF south of 60°S for Antarctica). Column 5: seasonal minimum LIG sea ice area (mill. km^2). Column 6: LIG-PI anomaly in seasonal minimum SIA (in %).

Simulation	Annual ΔSAT	Annual SIA (mill km^2)	Annual ΔSIA (%)	Summer ΔSAT	Monthly minimum SIA (mill km^2)	Monthly minimum ΔSIA (%)
			Arctic			
MPI-ESM-wiso$_{127k}$	0.4	11.6	-6.9	1.8	2.7	-55. 0
GISS$_{127k}$	0.91	15.4	-5.1	2.69	6.4	-34.5
HadCM3$_{127k}$	-0.32	8.9	-0.8	1.67	1.7	-40.8
H11-200	-2.68	10.9	21.5	0.82	2.3	-22.9
H11-3000	-1.51	9.9	10.5	1.23	1.8	-38. 0
H11-overshoot	2.18	7.1	-20.7	3.02	0.7	-74.7
			Antarctic			
MPI-ESM-wiso$_{127k}$	0.84	4.4	-23.7	-0.77	0.5	-6.8
GISS$_{127k}$	0.01	8.7	-2.4	-0.02	1.6	48.4
HadCM3$_{127k}$	0.45	10.4	-3.2	-1.64	3. 0	24.5
H11-200	1.95	8.4	-21.8	-5.58	2. 0	-17.3
H11-3000	3.12	6.7	-37.3	-3.76	1.4	-42.1
H11-overshoot	2.52	7.6	-29.7	1.79	1.7	-27.4

Table A4. Simulated Southern Ocean SST and sea ice values, and comparison with equivalent observational syntheses from Gao et al. (2024a). Left-most columns show average annual and summer ΔSST, for the Southen Ocean (south of 40°S) for each simulation. Right columns show SST synthesis averages (top row) as compiled by Gao et al. (2024a). Lower rows show the percentage of the observed core-site ΔSST values achieved by each simulation, for each data synthesis. See text and Gao et al. (2024a) for details of data synthesis.

			EC2017		JH2017		DC2021		MC2021	
	Annual ΔSST	Summer ΔSST	Annual ΔSST	Summer ΔSST	Annual ΔSST	Summer ΔSST	Annual ΔSST	Summer ΔSST	Summer ΔSST	September ΔSIA (%)
Synthesis mean	-	-	4.0K	1.7K	2.6K	1.7K	2.2K	2.2K	1.2K	-41.3
			% of change captured by each simulation							
MPI-ESM-wiso$_{127k}$	0.26	-0.11	6.4	-6.1	10.2	-6.4	12.1	-4.8	-8.5	63.3
GISS$_{127k}$	-0.03	-0.38	-0.7	-21.8	-1.1	-22.9	-1.3	-17.1	-30.7	10.2
HadCM3$_{127k}$	0.14	-0.12	3.5	-6.7	5.6	-7.1	6.6	-5.3	-9.5	9.9
H11-200	0.89	0.76	21.9	43.7	34.6	46. 0	41. 0	34.4	61.6	49.2
H11-3000	1.38	1.28	34.2	73.5	53.9	77.2	63.9	57.7	103.4	83.2
H11-overshoot	0.95	0.87	23.6	49.6	37.2	52.1	44.2	39. 0	69.8	67.4

Table A5. Fits and projected ΔSAT values based on ice core $\Delta\delta^{18}O$, as Table 2, but based solely on the LIG$_{127k}$ simulations (H11 results excluded).

Site	Slope K per ‰	STDERR K per ‰	Projected SAT K
	Arctic core sites		
NEEM	0.44	0.16	1.58 ± 2.65
NGRIP	0.26	0.24	0.81 ± 3.5
GRIP	0.30	0.26	0.97 ± 4.04
GISP2	0.31	0.28	0.84 ± 3.76
Camp_century	-0.10	0.17	-0.2 ± 1.74
DYE3	1.74	0.31	8.19 ± 6.37
	Antarctic core sites		
Vostok	-0.77	0.53	-2.54 ± 7.67
Dome F	0.81	0.31	3.63 ± 6.11
EDC	1.36	1.36	5.42 ± 23.61
EDML	0.28	0.32	0.82 ± 4.43
TALDICE	0.08	0.16	0.25 ± 3.65
Taylor	0.09	0.35	0.18 ± 4.91

Table A6. Fits and projected ΔSAT values based on ice core $\Delta\delta^{18}O$, as Table 2, but based solely on the H11 simulations (LIG_{127k} results excluded).

Site	Slope	STDERR	Projected SAT
	K per ‰	K per ‰	K
	Arctic core sites		
NEEM	0.85	0.12	3.05 ± 2.65
NGRIP	1.17	0.10	3.63 ± 2.22
GRIP	1.20	0.15	3.83 ± 3.56
GISP2	1.17	0.11	3.16 ± 2.66
Camp_century	0.82	0.10	1.63 ± 2.09
DYE3	0.55	0.14	2.61 ± 6.06
	Antarctic core sites		
Vostok	1.13	0.07	3.72 ± 1.41
Dome F	0.97	0.05	4.38 ± 1.21
EDC	1.09	0.07	4.38 ± 1.69
EDML	0.96	0.03	2.79 ± 0.77
TALDICE	0.93	0.07	2.96 ± 1.77
Taylor	0.82	0.11	1.57 ± 2.12

Table A7. This table is as 2, but using a two-part regression, *i.e.* allowing non-zero intercepts. Both the gradient and the intercept are used in the calculation of the projected temperature.

Site	Slope K per ‰	Intercept K	STDERR K per ‰	Projected SAT K
		Arctic core sites		
NGRIP	1.1	-0.43	0.1	2.97 ± 1.51
GRIP	1.11	-0.66	0.09	2.88 ± 1.48
GISP2	1.09	-0.52	0.09	2.41 ± 1.46
Camp_century	0.73	-0.5	0.08	0.98 ± 1.21
DYE3	0.63	0.58	0.09	3.56 ± 2.67
		Antarctic core sites		
Vostok	0.77	0.71	0.11	3.24 ± 1.22
Dome F	0.98	-0.03	0.09	4.39 ± 1.00
EDC	0.94	0.4	0.1 0	4.14 ± 1.23
EDML	1.19	-0.71	0.14	2.73 ± 1.22
TALDICE	0.43	1.13	0.07	2.52 ± 1.36
Taylor	0.45	0.93	0.05	1.78 ± 0.68

Author contributions. LCS led the development of this study. RS, MW, AC, and ANL ran simulations. RS performed all data analysis. LCS wrote the first draft of this manuscript. All authors contributed to the final draft.

Competing interests. Some authors are members of the editorial board of Climate of the Past.

Acknowledgements. LCS is supported in this work through: Past-to-Future: Towards fully paleo-informed future climate projections (P2F), GN 101184070; The Sensitivity of the West Antarctic Ice Sheet to +2C: SWAIS2C, NE/X009386/1. Assessing ocean-forced, marine-terminating glacier change in Greenland during climatic warm periods and its impact on marine productivity: KANG-GLAC, NE/V006509/1. EMcC, LCS, and RS are supported through European Research Council H2020 Grant Number 864637 (ANTarctic Sea Ice Evolution from a novel biological archive, ANTSIE). AdB is supported through Swedish Research Council grant VR 2020-04791.ANL thanks NASA High-End Computing Program for computing resources through the NASA Center for Climate Simulation at Goddard Space Flight Center and NASA GISS for institutional support, particularly interns of the NASA Climate Change Research Initiative program. AC and MW were supported by the German Federal Ministry of Education and Research (BMBF) as a Research for Sustainability initiative (FONA). MPI-ESM-wiso simulation was performed at the German Climate Computing Center (DKRZ).

References

Bakker, P., Masson-Delmotte, V., Martrat, B., Charbit, S., Renssen, H., Gröger, M., Krebs-Kanzow, U., Lohman, G., Lunt, D. J., Pfeiffer, M., Phipps, S. J., Prange, M., Ritz, S. P., Schulz, M., Stenni, B., Stone, E. J., and Varma, V.: Temperature trends during the present and last interglacial periods - a multi-model-data comparison, Quaternary Science Reviews, 99, https://doi.org/10.1016/j.quascirev.2014.06.031, 2014.

Bazin, L., Landais, A., Lemieux-Dudon, B., Toyé Mahamadou Kele, H., Veres, D., Parrenin, F., Martinerie, P., Ritz, C., Capron, E., Lipenkov, V., Loutre, M. F., Raynaud, D., Vinther, B., Svensson, A., Rasmussen, S. O., Severi, M., Blunier, T., Leuenberger, M., Fischer, H., Masson-Delmotte, V., Chappellaz, J., and Wolff, E.: An optimized multi-proxy, multi-site Antarctic ice and gas orbital chronology (AICC2012): 120-800 ka, Climate of the Past, 9, 1715–1731, https://doi.org/10.5194/CP-9-1715-2013, 2013.

Berger, A. and Loutre, M. F.: Insolation values for the climate of the last 10 million years, Quaternary Science Reviews, 10, 297–317, https://doi.org/10.1016/0277-3791(91)90033-Q, 1991.

Bertler, N. A., Conway, H., Dahl-Jensen, D., Emanuelsson, D. B., Winstrup, M., Vallelonga, P. T., Lee, J. E., Brook, E. J., Severinghaus, J. P., Fudge, T. J., Keller, E. D., Troy Baisden, W., Hindmarsh, R. C., Neff, P. D., Blunier, T., Edwards, R., Mayewski, P. A., Kipfstuhl, S., Buizert, C., Canessa, S., Dadic, R., Kjær, H. A., Kurbatov, A., Zhang, D., Waddington, E. D., Baccolo, G., Beers, T., Brightley, H. J., Carter, L., Clemens-Sewall, D., Ciobanu, V. G., Delmonte, B., Eling, L., Ellis, A., Ganesh, S., Golledge, N. R., Haines, S., Handley, M., Hawley, R. L., Hogan, C. M., Johnson, K. M., Korotkikh, E., Lowry, D. P., Mandeno, D., McKay, R. M., Menking, J. A., Naish, T. R., Noerling, C., Ollive, A., Orsi, A., Proemse, B. C., Pyne, A. R., Pyne, R. L., Renwick, J., Scherer, R. P., Semper, S., Simonsen, M., Sneed, S. B., Steig, E. J., Tuohy, A., Ulayottil Venugopal, A., Valero-Delgado, F., Venkatesh, J., Wang, F., Wang, S., Winski, D. A., Holly, W., Whiteford, A., Xiao, C., Yang, J., and Zhang, X.: The Ross Sea Dipole-temperature, snow accumulation and sea ice variability in the Ross Sea region, Antarctica, over the past 2700 years, https://doi.org/10.5194/cp-14-193-2018, 2018.

Boyle, E. A.: Cool tropical temperatures shift the global δ18O-T relationship: An explanation for the ice core δ18O-borehole thermometry conflict?, Geophysical Research Letters, 24, 273–276, 1997.

Buizert, C., Fudge, T., Roberts, W. H., Steig, E. J., Sherriff-Tadano, S., Ritz, C., Lefebvre, E., Edwards, J., Kawamura, K., Oyabu, I., et al.: Antarctic surface temperature and elevation during the Last Glacial Maximum, Science, 372, 1097–1101, 2021.

CAPE-Last Interglacial Project Members: Last Interglacial Arctic warmth confirms polar amplification of climate change, Quaternary Science Reviews, 25, 1383–1400, https://doi.org/10.1016/J.QUASCIREV.2006.01.033, 2006.

Capron, E., Govin, A., Stone, E. J., Masson-Delmotte, V., Mulitza, S., Otto-Bliesner, B., Rasmussen, T. L., Sime, L. C., Waelbroeck, C., and Wolff, E. W.: Temporal and spatial structure of multi-millennial temperature changes at high latitudes during the Last Interglacial, Quaternary Science Reviews, 103, 116–133, https://doi.org/10.1016/J.QUASCIREV.2014.08.018, 2014.

Capron, E., Govin, A., Feng, R., Otto-Bliesner, B. L., and Wolff, E. W.: Critical evaluation of climate syntheses to benchmark CMIP6/PMIP4 127 ka Last Interglacial simulations in the high-latitude regions, Quaternary Science Reviews, 168, 137–150, https://doi.org/10.1016/J.QUASCIREV.2017.04.019, 2017.

Cauquoin, A., Werner, M., and Lohmann, G.: Water isotopes – climate relationships for the mid-Holocene and preindustrial period simulated with an isotope-enabled version of MPI-ESM, Climate of the Past, 15, 1913–1937, https://doi.org/10.5194/cp-15-1913-2019, 2019.

Cauquoin, A., Abe-Ouchi, A., Obase, T., Chan, W. L., Paul, A., and Werner, M.: Effects of Last Glacial Maximum (LGM) sea surface temperature and sea ice extent on the isotope-temperature slope at polar ice core sites, Climate of the Past, 19, https://doi.org/10.5194/cp-19-1275-2023, 2023.

Chadwick, M., Allen, C. S., Sime, L. C., and Hillenbrand, C. D.: Analysing the timing of peak warming and minimum winter sea-ice extent in the Southern Ocean during MIS 5e, Quaternary Science Reviews, 229, 106 134, https://doi.org/10.1016/J.QUASCIREV.2019.106134, 2020.

Chadwick, M., Allen, C. S., and Crosta, X.: MIS 5e Southern Ocean September sea-ice concentrations and summer sea-surface temperatures reconstructed from marine sediment cores using a MAT diatom transfer function, https://doi.org/10.1594/PANGAEA.936573, 2021.

Chadwick, M., Crosta, X., Esper, O., Thöle, L., and Kohfeld, K. E.: Compilation of Southern Ocean sea-ice records covering the last glacial-interglacial cycle (12-130ka), Climate of the Past, 18, 1815–1829, https://doi.org/10.5194/CP-18-1815-2022, 2022.

Chadwick, M., Sime, L. C., Allen, C. S., and Guarino, M.: Model-Data Comparison of Antarctic Winter Sea-Ice Extent and Southern Ocean Sea-Surface Temperatures During Marine Isotope Stage 5e, Paleoceanography and Paleoclimatology, 38, https://doi.org/10.1029/2022pa004600, 2023.

Chandler, D. and Langebroek, P.: Southern Ocean sea surface temperature synthesis: Part 2. Penultimate glacial and last interglacial, Quaternary Science Reviews, 271, 107 190, https://doi.org/10.1016/J.QUASCIREV.2021.107190, 2021.

Clark, P. U., Pisias, N. G., Stocker, T. F., and Weaver, A. J.: The role of the thermohaline circulation in abrupt climate change, Nature, 415, 863–869, 2002.

Claussen, M., Fohlmeister, J., Ganopolski, A., and Brovkin, V.: Vegetation dynamics amplifies precessional forcing, Geophysical Research Letters, 33, 2006.

Crosta, X., Kohfeld, K. E., Bostock, H. C., Chadwick, M., Vivier, A. D., Esper, O., Etourneau, J., Jones, J., Leventer, A., Müller, J., Rhodes, R. H., Allen, C. S., Ghadi, P., Lamping, N., Lange, C. B., Lawler, K. A., Lund, D., Marzocchi, A., Meissner, K. J., Menviel, L., Nair, A., Patterson, M., Pike, J., Prebble, J. G., Riesselman, C., Sadatzki, H., Sime, L. C., Shukla, S. K., Thöle, L., Vorrath, M. E., Xiao, W., and Yang, J.: Antarctic sea ice over the past 130 000 years - Part 1: a review of what proxy records tell us, Climate of the Past, 18, 1729–1756, https://doi.org/10.5194/CP-18-1729-2022, 2022.

Dansgaard, W.: The O18-abundance in fresh water, Geochimica et Cosmochimica Acta, 6, 241–260, 1954.

Delaygue, G., Jouzel, J., Masson, V., Koster, R. D., and Bard, E.: Validity of the isotopic thermometer in central Antarctica: Limited impact of glacial precipitation seasonality and moisture origin., Geophysical Research Letters, 27, https://doi.org/10.1029/2000GL011530, 2000.

Diamond, R., Sime, L. C., Schroeder, D., and Guarino, M. V.: The contribution of melt ponds to enhanced Arctic sea-ice melt during the Last Interglacial, Cryosphere, 15, 5099–5114, https://doi.org/10.5194/TC-15-5099-2021, 2021.

Diamond, R., Schroeder, D., Sime, L. C., Ridley, J., and Feltham, D.: The Significance of the Melt-Pond Scheme in a CMIP6 Global Climate Model, Journal of Climate, 37, 249–268, https://doi.org/10.1175/JCLI-D-22-0902.1, 2023.

Domingo, D., Malmierca-Vallet, I., Sime, L., Voss, J., and Capron, E.: Using Ice Cores and Gaussian Process Emulation to Recover Changes in the Greenland Ice Sheet During the Last Interglacial, Journal of Geophysical Research: Earth Surface, 125, https://doi.org/10.1029/2019JF005237, 2020.

EPICA community members: Eight glacial cycles from an Antarctic ice core, Nature, 429, 623–628, https://doi.org/10.1038/nature02599, 2004.

EPICA Community Members: One-to-one coupling of glacial climate variability in Greenland and Antarctica, Nature, 444, https://doi.org/10.1038/nature05301, 2006.

Eyring, V., Bony, S., Meehl, G. A., Senior, C. A., Stevens, B., Stouffer, R. J., and Taylor, K. E.: Overview of the Coupled Model Intercomparison Project Phase 6 (CMIP6) experimental design and organization, Geoscientific Model Development, 9, 1937–1958, https://doi.org/10.5194/GMD-9-1937-2016, 2016.

Fischer, H., Meissner, K. J., Mix, A. C., Abram, N. J., Austermann, J., Brovkin, V., Capron, E., Colombaroli, D., Daniau, A. L., Dyez, K. A., Felis, T., Finkelstein, S. A., Jaccard, S. L., McClymont, E. L., Rovere, A., Sutter, J., Wolff, E. W., Affolter, S., Bakker, P., Ballesteros-Cánovas, J. A., Barbante, C., Caley, T., Carlson, A. E., Churakova, O., Cortese, G., Cumming, B. F., Davis, B. A., De Vernal, A., Emile-Geay, J., Fritz, S. C., Gierz, P., Gottschalk, J., Holloway, M. D., Joos, F., Kucera, M., Loutre, M. F., Lunt, D. J., Marcisz, K., Marlon, J. R., Martinez, P., Masson-Delmotte, V., Nehrbass-Ahles, C., Otto-Bliesner, B. L., Raible, C. C., Risebrobakken, B., Sánchez Goñi, M. F., Arrigo, J. S., Sarnthein, M., Sjolte, J., Stocker, T. F., Velasquez Alvárez, P. A., Tinner, W., Valdes, P. J., Vogel, H., Wanner, H., Yan, Q., Yu, Z., Ziegler, M., and Zhou, L.: Palaeoclimate constraints on the impact of 2 °c anthropogenic warming and beyond, https://doi.org/10.1038/s41561-018-0146-0, 2018.

Gao, Q., Capron, E., Sime, L. C., Rhodes, R. H., Sivankutty, R., Zhang, X., Otto-Bliesner, B. L., and Werner, M.: Assessment of the southern polar and subpolar warming in the PMIP4 Last Interglacial simulations using paleoclimate data syntheses, EGUsphere, 2024, 1–32, https://doi.org/10.5194/egusphere-2024-1261, 2024a.

Gao, Q., Sime, L. C., McLaren, A. J., Bracegirdle, T. J., Capron, E., Rhodes, R. H., Steen-Larsen, H. C., Shi, X., and Werner, M.: Evaporative controls on Antarctic precipitation: an ECHAM6 model study using innovative water tracer diagnostics, The Cryosphere, 18, 683–703, 2024b.

Giorgetta, M. A., Jungclaus, J., Reick, C. H., Legutke, S., Bader, J., Böttinger, M., Brovkin, V., Crueger, T., Esch, M., Fieg, K., et al.: Climate and carbon cycle changes from 1850 to 2100 in MPI-ESM simulations for the Coupled Model Intercomparison Project phase 5, Journal of Advances in Modeling Earth Systems, 5, 572–597, 2013.

Golledge, N. R., Clark, P. U., He, F., Dutton, A., Turney, C. S., Fogwill, C. J., Naish, T. R., Levy, R. H., McKay, R. M., Lowry, D. P., Bertler, N. A., Dunbar, G. B., and Carlson, A. E.: Retreat of the Antarctic Ice Sheet During the Last Interglaciation and Implications for Future Change, Geophysical Research Letters, 48, e2021GL094 513, https://doi.org/10.1029/2021GL094513, 2021.

Goursaud, S., Holloway, M., Sime, L., Wolff, E., Valdes, P., Steig, E. J., and Pauling, A.: Antarctic Ice Sheet Elevation Impacts on Water Isotope Records During the Last Interglacial, https://doi.org/10.1029/2020GL091412, 2021.

Guan, J., Liu, Z., Wen, X., Brady, E., Noone, D., Zhu, J., and Han, J.: Understanding the temporal slope of the temperature-water isotope relation during the deglaciation using isoCAM3: The slope equation, Journal of Geophysical Research: Atmospheres, 121, 10–342, 2016.

Guarino, M. V., Sime, L. C., Schröeder, D., Malmierca-Vallet, I., Rosenblum, E., Ringer, M., Ridley, J., Feltham, D., Bitz, C., Steig, E. J., Wolff, E., Stroeve, J., and Sellar, A.: Sea-ice-free Arctic during the Last Interglacial supports fast future loss, Nature Climate Change 2020 10:10, 10, 928–932, https://doi.org/10.1038/s41558-020-0865-2, 2020.

Guarino, M. V., Sime, L. C., Diamond, R., Ridley, J., and Schroeder, D.: The coupled system response to 250 years of freshwater forcing: Last Interglacial CMIP6-PMIP4 HadGEM3 simulations, Climate of the Past, 19, 865–881, https://doi.org/10.5194/CP-19-865-2023, 2023.

Heinrich, H.: Origin and consequences of cyclic ice rafting in the northeast Atlantic Ocean during the past 130,000 years, Quaternary research, 29, 142–152, 1988.

Hemming, S. R.: Heinrich events: Massive late Pleistocene detritus layers of the North Atlantic and their global climate imprint, Reviews of Geophysics, 42, 2004.

Hoffman, J. S., Clark, P. U., Parnell, A. C., and He, F.: Regional and global sea-surface temperatures during the last interglaciation, Science, 355, 276–279, https://doi.org/10.1126/science.aai8464, 2017.

Holloway, M. D., Sime, L. C., Singarayer, J. S., Tindall, J. C., Bunch, P., and Valdes, P. J.: Antarctic last interglacial isotope peak in response to sea ice retreat not ice-sheet collapse, Nature Communications 2016 7:1, 7, 1–9, https://doi.org/10.1038/ncomms12293, 2016.

Holloway, M. D., Sime, L. C., Allen, C. S., Hillenbrand, C. D., Bunch, P., Wolff, E., and Valdes, P. J.: The Spatial Structure of the 128 ka Antarctic Sea Ice Minimum, Geophysical Research Letters, 44, 129–11, https://doi.org/10.1002/2017GL074594, 2017.

Holloway, M. D., Sime, L. C., Singarayer, J. S., Tindall, J. C., and Valdes, P. J.: Simulating the 128-ka Antarctic Climate Response to Northern Hemisphere Ice Sheet Melting Using the Isotope-Enabled HadCM3, Geophysical Research Letters, 45, 921–11, https://doi.org/10.1029/2018GL079647, 2018.

Hutchinson, D. K., Menviel, L., Meissner, K. J., and Hogg, A. M.: East Antarctic warming forced by ice loss during the Last Interglacial, Nature Communications, 15, 1026, 2024.

IPCC: Climate Change 2021: The Physical Science Basis. Contribution of Working Group I to the Sixth Assessment Report of the Intergovernmental Panel on Climate Change, vol. In Press, Cambridge University Press, Cambridge, United Kingdom and New York, NY, USA, https://doi.org/10.1017/9781009157896, 2021.

Johnsen, S. J., Dahl-Jensen, D., Gundestrup, N., Steffensen, J. P., Clausen, H. B., Miller, H., Masson-Delmotte, V., Sveinbjörnsdottir, A. E., and White, J.: Oxygen isotope and palaeotemperature records from six Greenland ice-core stations: Camp Century, Dye-3, GRIP, GISP2, Renland and NorthGRIP, Journal of Quaternary Science, 16, 299–307, https://doi.org/https://doi.org/10.1002/jqs.622, 2001.

Jouzel, J., Alley, R., Cuffey, K., Dansgaard, W., Grootes, P., Hoffmann, G., Johnsen, S., Koster, R., Peel, D., Shuman, C., et al.: Validity of the temperature reconstruction from water isotopes in ice cores, Journal of Geophysical Research: Oceans, 102, 26 471–26 487, 1997.

Jouzel, J., Vimeux, F., Caillon, N., Delaygue, G., Hoffmann, G., Masson-Delmotte, V., and Parrenin, F.: Magnitude of isotope/temperature scaling for interpretation of central Antarctic ice cores, Journal of Geophysical Research: Atmospheres, 108, 4361, https://doi.org/10.1029/2002JD002677, 2003.

Jouzel, J., Masson-Delmotte, V., Cattani, O., Dreyfus, G., Falourd, S., Hoffmann, G., Minster, B., Nouet, J., Barnola, J. M., Chappellaz, J., Fischer, H., Gallet, J. C., Johnsen, S., Leuenberger, M., Loulergue, L., Luethi, D., Oerter, H., Parrenin, F., Raisbeck, G., Raynaud, D., Schilt, A., Schwander, J., Selmo, E., Souchez, R., Spahni, R., Stauffer, B., Steffensen, J. P., Stenni, B., Stocker, T. F., Tison, J. L., Werner, M., and Wolff, E. W.: Orbital and millennial antarctic climate variability over the past 800,000 years, Science, 317, 793–796, https://doi.org/10.1126/science.1141038, 2007.

Kageyama, M., Harrison, S. P., Kapsch, M. L., Lofverstrom, M., Lora, J. M., Mikolajewicz, U., Sherriff-Tadano, S., Vadsaria, T., Abe-Ouchi, A., Bouttes, N., Chandan, D., Gregoire, L. J., Ivanovic, R. F., Izumi, K., Legrande, A. N., Lhardy, F., Lohmann, G., Morozova, P. A., Ohgaito, R., Paul, A., Richard Peltier, W., Poulsen, C. J., Quiquet, A., Roche, D. M., Shi, X., Tierney, J. E., Valdes, P. J., Volodin, E., and Zhu, J.: The PMIP4 Last Glacial Maximum experiments: Preliminary results and comparison with the PMIP3 simulations, Climate of the Past, 17, 1065–1089, https://doi.org/10.5194/CP-17-1065-2021, 2021.

Kawamura, K., Parrenin, F., Lisiecki, L., Uemura, R., Vimeux, F., Severinghaus, J. P., Hutterli, M. A., Nakazawa, T., Aoki, S., Jouzel, J., Raymo, M. E., Matsumoto, K., Nakata, H., Motoyama, H., Fujita, S., Goto-Azuma, K., Fujii, Y., and Watanabe, O.: Northern Hemisphere forcing of climatic cycles in Antarctica over the past 360,000 years, Nature, 448, https://doi.org/10.1038/nature06015, 2007.

Kelley, M., Schmidt, G. A., Nazarenko, L. S., Bauer, S. E., Ruedy, R., Russell, G. L., Ackerman, A. S., Aleinov, I., Bauer, M., Bleck, R., et al.: GISS-E2. 1: Configurations and climatology, Journal of Advances in Modeling Earth Systems, 12, e2019MS002 025, 2020.

Kindler, P., Guillevic, M., Baumgartner, M., Schwander, J., Landais, A., and Leuenberger, M.: Temperature reconstruction from 10 to 120 kyr b2k from the NGRIP ice core, Climate of the Past, 10, 887–902, 2014.

Krinner, G., Genthon, C., and Jouzel, J.: GCM analysis of local influences on ice core δ signals, Geophysical Research Letters, 24, https://doi.org/10.1029/97GL52891, 1997.

Landais, A., Chappellaz, J., Delmotte, M., Jouzel, J., Blunier, T., Bourg, C., Caillon, N., Cherrier, S., Malaizé, B., Masson-Delmotte, V., Raynaud, D., Schwander, J., and Steffensen, J. P.: A tentative reconstruction of the last interglacial and glacial inception in Greenland based on new gas measurements in the Greenland Ice Core Project (GRIP) ice core, Journal of Geophysical Research: Atmospheres, 108, https://doi.org/https://doi.org/10.1029/2002JD003147, 2003.

Lee, J.-E., Fung, I., DePaolo, D. J., and Otto-Bliesner, B.: Water isotopes during the Last Glacial Maximum: New general circulation model calculations, Journal of Geophysical Research: Atmospheres, 113, 2008.

Liu, Z., He, C., Yan, M., Buizert, C., Otto-Bliesner, B., Lu, F., and Zeng, C.: Reconstruction of Past Antarctic Temperature Using Present Seasonal δ18O–Inversion Layer Temperature: Unified Slope Equations and Applications, Journal of Climate, 36, 2023.

Lunt, D. J., Abe-Ouchi, A., Bakker, P., Berger, A., Braconnot, P., Charbit, S., Fischer, N., Herold, N., Jungclaus, J. H., Khon, V. C., Krebs-Kanzow, U., Langebroek, P. M., Lohmann, G., Nisancioglu, K. H., Otto-Bliesner, B. L., Park, W., Pfeiffer, M., Phipps, S. J., Prange, M., Rachmayani, R., Renssen, H., Rosenbloom, N., Schneider, B., Stone, E. J., Takahashi, K., Wei, W., Yin, Q., and Zhang, Z. S.: A multi-model assessment of last interglacial temperatures, Climate of the Past, 9, 699–717, https://doi.org/10.5194/CP-9-699-2013, 2013.

Malmierca-Vallet, I., Sime, L. C., Tindall, J. C., Capron, E., Valdes, P. J., Vinther, B. M., and Holloway, M. D.: Simulating the Last Interglacial Greenland stable water isotope peak: The role of Arctic sea ice changes, Quaternary Science Reviews, 198, 1–14, 2018.

Marino, G., Rohling, E., Rodríguez-Sanz, L., Grant, K., Heslop, D., Roberts, A., Stanford, J., and Yu, J.: Bipolar seesaw control on last interglacial sea level, Nature, 522, 197–201, 2015.

Masson-Delmotte, V., Dreyfus, G., Braconnot, P., Johnsen, S., Jouzel, J., Kageyama, M., Landais, A., Loutre, M.-F., Nouet, J., Parrenin, F., et al.: Past temperature reconstructions from deep ice cores: relevance for future climate change, Climate of the Past, 2, 145–165, 2006.

Masson-Delmotte, V., Buiron, D., Ekaykin, A., Frezzotti, M., Gallée, H., Jouzel, J., Krinner, G., Landais, A., Motoyama, H., Oerter, H., Pol, K., Pollard, D., Ritz, C., Schlosser, E., Sime, L. C., Sodemann, H., Stenni, B., Uemura, R., and Vimeux, F.: A comparison of the present and last interglacial periods in six Antarctic ice cores, Climate of the Past, 7, 397–423, https://doi.org/10.5194/CP-7-397-2011, 2011.

Mauritsen, T., Bader, J., Becker, T., Behrens, J., Bittner, M., Brokopf, R., Brovkin, V., Claussen, M., Crueger, T., Esch, M., et al.: Developments in the MPI-M Earth System Model version 1.2 (MPI-ESM1. 2) and its response to increasing CO2, Journal of Advances in Modeling Earth Systems, 11, 998–1038, 2019.

McLaren, A. J., Sime, L. C., Wilson, S., Ridley, J., Gao, Q., Gorguner, M., Line, G., Werner, M., and Valdes, P.: Implementation of Water Tracers in the Met Office Unified Model, EGUsphere, 2025, 1–25, 2025.

McManus, J. F., Francois, R., Gherardi, J.-M., Keigwin, L. D., and Brown-Leger, S.: Collapse and rapid resumption of Atlantic meridional circulation linked to deglacial climate changes, nature, 428, 834–837, 2004.

Members, North Greenland Ice Core Project: High-resolution record of Northern Hemisphere climate extending into the last interglacial period, Nature, 431, 147–151, https://doi.org/10.1038/nature02805, 2004.

Münch, T., Werner, M., and Laepple, T.: How precipitation intermittency sets an optimal sampling distance for temperature reconstructions from Antarctic ice cores, Climate of the Past Discussions, 2020, 1–24, 2020.

NEEM community members: Eemian interglacial reconstructed from a Greenland folded ice core, Nature, 493, https://doi.org/10.1038/nature11789, 2013.

Nikolova, I., Yin, Q., Berger, A., Singh, U. K., and Karami, M. P.: The last interglacial (Eemian) climate simulated by LOVECLIM and CCSM3, Climate of the Past, 9, 1789–1806, 2013.

Noone, D. and Simmonds, I.: Annular variations in moisture transport mechanisms and the abundance of δ18O in Antarctic snow, Journal of Geophysical Research: Atmospheres, 107, 3–1, https://doi.org/10.1029/2002JD002262, 2002.

Oger, S., Sime, L., and Holloway, M.: Decoupling of $\delta^{18}O$ from surface temperature in Antarctica in an ensemble of Historical simulations, EGUsphere, 2023, 1–29, https://doi.org/10.5194/egusphere-2023-2735, 2023.

Otto-Bliesner, B. L., Marshall, S. J., Overpeck, J. T., Miller, G. H., Hu, A., and members, C. L. I. P.: Simulating Arctic climate warmth and icefield retreat in the last interglaciation, science, 311, 1751–1753, 2006.

Otto-Bliesner, B. L., Rosenbloom, N., Stone, E. J., Mckay, N. P., Lunt, D. J., Brady, E. C., and Overpeck, J. T.: How warm was the last interglacial? New model-data comparisons, Philosophical Transactions of the Royal Society A: Mathematical, Physical and Engineering Sciences, 371, https://doi.org/10.1098/RSTA.2013.0097, 2013.

Otto-Bliesner, B. L., Braconnot, P., Harrison, S. P., Lunt, D. J., Abe-Ouchi, A., Albani, S., Bartlein, P. J., Capron, E., Carlson, A. E., Dutton, A., Fischer, H., Goelzer, H., Govin, A., Haywood, A., Joos, F., Legrande, A. N., Lipscomb, W. H., Lohmann, G., Mahowald, N., Nehrbass-Ahles, C., Pausata, F. S., Peterschmitt, J. Y., Phipps, S. J., Renssen, H., and Zhang, Q.: The PMIP4 contribution to CMIP6 - Part 2: Two interglacials, scientific objective and experimental design for Holocene and Last Interglacial simulations, Geoscientific Model Development, 10, 3979–4003, https://doi.org/10.5194/GMD-10-3979-2017, 2017.

Otto-Bliesner, B. L., Brady, E. C., Zhao, A., Brierley, C. M., Axford, Y., Capron, E., Govin, A., Hoffman, J. S., Isaacs, E., Kageyama, M., Scussolini, P., Tzedakis, P. C., Williams, C. J., Wolff, E., Abe-Ouchi, A., Braconnot, P., Ramos Buarque, S., Cao, J., De Vernal, A., Vittoria Guarino, M., Guo, C., Legrande, A. N., Lohmann, G., Meissner, K. J., Menviel, L., Morozova, P. A., Nisancioglu, K. H., O'Ishi, R., Mélia, D. S. Y., Shi, X., Sicard, M., Sime, L., Stepanek, C., Tomas, R., Volodin, E., Yeung, N. K., Zhang, Q., Zhang, Z., and Zheng, W.: Large-scale features of Last Interglacial climate: Results from evaluating the lig127k simulations for the Coupled Model Intercomparison Project (CMIP6)-Paleoclimate Modeling Intercomparison Project (PMIP4), Climate of the Past, 17, 63–94, https://doi.org/10.5194/cp-17-63-2021, 2021.

Past Interglacials Working Group of PAGES: Interglacials of the last 800,000 years, https://doi.org/10.1002/2015RG000482, 2016.

Petit, J. R., Jouzel, J., Raynaud, D., Barkov, N. I., Barnola, J. M., Basile, I., Bender, M., Chappellaz, J., Davis, M., Delaygue, G., Delmotte, M., Kotiyakov, V. M., Legrand, M., Lipenkov, V. Y., Lorius, C., Pépin, L., Ritz, C., Saltzman, E., and Stievenard, M.: Climate and atmospheric history of the past 420,000 years from the Vostok ice core, Antarctica, Nature, 399, 429–436, https://doi.org/10.1038/20859, 1999.

Rahmstorf, S.: The thermohaline ocean circulation-a system with dangerous thresholds?, Climatic Change, 46, 247–256, 2000.

Razmjooei, M. J., Henderiks, J., Coxall, H. K., Baumann, K.-H., Vermassen, F., Jakobsson, M., Niessen, F., and O'Regan, M.: RevisionoftheQuaternarycalcareousnannofossilbiochronologyofArcticOceansediments, QuaternaryScienceReviews, 321, 10838

Schlosser, E., Reijmer, C., Oerter, H., and Graf, W.: The influence of precipitation origin on the $\delta^{18}O$-T relationship at Neumayer station, Ekströmisen, Antarctica, Annals of Glaciology, 39, https://doi.org/10.3189/172756404781814276, 2004.

Schurgers, G., Mikolajewicz, U., Gröger, M., Maier-Reimer, E., Vizcaíno, M., and Winguth, A.: The effect of land surface changes on Eemian climate, Climate dynamics, 29, 357–373, 2007.

Seabold, S. and Perktold, J.: statsmodels: Econometric and statistical modeling with python, in: 9th Python in Science Conference, 2010.

Shackleton, S., Baggenstos, D., Menking, J. A., Dyonisius, M. N., Bereiter, B., Bauska, T. K., Rhodes, R. H., Brook, E. J., Petrenko, V. V., McConnell, J. R., Kellerhals, T., Häberli, M., Schmitt, J., Fischer, H., and Severinghaus, J. P.: Global ocean heat content in the Last Interglacial, Nature Geoscience, 13, 77–81, https://doi.org/10.1038/s41561-019-0498-0, 2020.

Sime, L. C., Tindall, J. C., Wolff, E. W., Connolley, W. M., and Valdes, P. J.: Antarctic isotopic thermometer during a CO2 forced warming event, Journal of Geophysical Research, 113, D24 119, https://doi.org/10.1029/2008JD010395, 2008.

Sime, L. C., Wolff, E. W., Oliver, K. I., and Tindall, J. C.: Evidence for warmer interglacials in East Antarctic ice cores, Nature, 462, 342–345, https://doi.org/10.1038/nature08564, 2009.

Sime, L. C., Risi, C., Tindall, J. C., Sjolte, J., Wolff, E. W., Masson-Delmotte, V., and Capron, E.: Warm climate isotopic simulations: what do we learn about interglacial signals in Greenland ice cores?, Quaternary Science Reviews, 67, 59–80, 2013.

Sime, L. C., Carlson Anders E., and Holloway, M. D.: On recovering Last Interglacial changes in the Antarctic ice sheet, Past Global Changes Magazine, 27, https://doi.org/10.22498/pages.27.1.14, 2019a.

Sime, L. C., Hopcroft, P. O., and Rhodes, R. H.: Impact of abrupt sea ice loss on Greenland water isotopes during the last glacial period, Proceedings of the National Academy of Sciences, 116, 4099–4104, 2019b.

Sime, L. C., Sivankutty, R., Vallet-Malmierca, I., de Boer, A. M., and Sicard, M.: Summer surface air temperature proxies point to near-sea-ice-free conditions in the Arctic at 127 ka, Climate of the Past, 19, 883–900, https://doi.org/10.5194/cp-19-883-2023, 2023.

Sjolte, J., Hoffmann, G., and Johnsen, S. J.: Modelling the response of stable water isotopes in Greenland precipitation to orbital configurations of the previous interglacial, Tellus B: Chemical and Physical Meteorology, 66, 22 872, 2014.

Steig, E. J., Morse, D. L., Waddington, E. D., Stuiver, M., Grootes, P. M., Mayewski, P. A., Twickler, M. S., and Whitlow, S. I.: Wisconsinan and Holocene Climate History from an Ice Core at Taylor Dome, Western Ross Embayment, Antarctica, Geografiska Annaler, Series A: Physical Geography, 82A, https://doi.org/10.1111/1468-0459.00122, 2000.

Stenni, B., Buiron, D., Frezzotti, M., Albani, S., Barbante, C., Bard, E., Barnola, J. M., Baroni, M., Baumgartner, M., Bonazza, M., Capron, E., Castellano, E., Chappellaz, J., Delmonte, B., Falourd, S., Genoni, L., Iacumin, P., Jouzel, J., Kipfstuhl, S., Landais, A., Lemieux-Dudon, B., Maggi, V., Masson-Delmotte, V., Mazzola, C., Minster, B., Montagnat, M., Mulvaney, R., Narcisi, B., Oerter, H., Parrenin, F., Petit, J. R., Ritz, C., Scarchilli, C., Schilt, A., Schüpbach, S., Schwander, J., Selmo, E., Severi, M., Stocker, T. F., and Udisti, R.: Expression of the bipolar see-saw in Antarctic climate records during the last deglaciation, Nature Geoscience, 4, https://doi.org/10.1038/ngeo1026, 2011.

Stoll, H. M., Cacho, I., Gasson, E., Sliwinski, J., Kost, O., Moreno, A., Iglesias, M., Torner, J., Perez-Mejias, C., Haghipour, N., et al.: Rapid northern hemisphere ice sheet melting during the penultimate deglaciation, Nature communications, 13, 3819, 2022.

Stone, E. J., Capron, E., Lunt, D. J., Payne, A. J., Singarayer, J. S., Valdes, P. J., and Wolff, E. W.: Impact of meltwater on high-latitude early Last Interglacial climate, Climate of the Past, 12, 1919–1932, https://doi.org/10.5194/CP-12-1919-2016, 2016.

Suwa, M. and Bender, M. L.: O_2/N_2 ratios of occluded air in the GISP2 ice core, Journal of Geophysical Research: Atmospheres, 113, https://doi.org/https://doi.org/10.1029/2007JD009589, 2008.

Tindall, J. C., Valdes, P. J., and Sime, L. C.: Stable water isotopes in HadCM3: Isotopic signature of El Niño–Southern Oscillation and the tropical amount effect, Journal of Geophysical Research: Atmospheres, 114, 4111, https://doi.org/10.1029/2008JD010825, 2009.

Vermassen, F., O'Regan, M., de Boer, A., Schenk, F., Razmjooei, M., West, G., Cronin, T. M., Jakobsson, M., and Coxall, H. K.: A seasonally ice-free Arctic Ocean during the Last Interglacial, Nature Geoscience, 16, 723–729, 2023.

Vimeux, F., Masson, V., Jouzel, J., Stievenard, M., and Petit, J. R.: Glacial-interglacial changes in ocean surface conditions in the Southern Hemisphere, Nature, 398, https://doi.org/10.1038/18860, 1999.

Vinther, B. M., Buchardt, S. L., Clausen, H. B., Dahl-Jensen, D., Johnsen, S. J., Fisher, D., Koerner, R., Raynaud, D., Lipenkov, V., Andersen, K. K., et al.: Holocene thinning of the Greenland ice sheet, Nature, 461, 385–388, 2009.

Vinther, B. M., Jones, P. D., Briffa, K., Clausen, H., Andersen, K. K., Dahl-Jensen, D., and Johnsen, S.: Climatic signals in multiple highly resolved stable isotope records from Greenland, Quaternary Science Reviews, 29, 522–538, 2010.

WAIS Divide Project Members: Precise interpolar phasing of abrupt climate change during the last ice age, Nature, 520, https://doi.org/10.1038/nature14401, 2015.

Weaver, A. J., Saenko, O. A., Clark, P. U., and Mitrovica, J. X.: Meltwater pulse 1A from Antarctica as a trigger of the Bølling-Allerød warm interval, Science, 299, 1709–1713, 2003.

Werner, M. and Heimann, M.: Modeling interannual variability of water isotopes in Greenland and Antarctica, Journal of Geophysical Research: Atmospheres, 107, 1–1, https://doi.org/10.1029/2001JD900253, 2002.

Werner, M., Heimann, M., and Hoffmann, G.: Isotopic composition and origin of polar precipitation in present and glacial climate simulations, Tellus B: Chemical and Physical Meteorology, 53, 53–71, https://doi.org/10.3402/TELLUSB.V53I1.16539, 2001.

Werner, M., Jouzel, J., Masson-Delmotte, V., and Lohmann, G.: Reconciling glacial Antarctic water stable isotopes with ice sheet topography and the isotopic paleothermometer, Nature Communications, 9, 1–10, https://doi.org/10.1038/s41467-018-05430-y, 2018.

Wolff, E. W., Fischer, H., Fundel, F., Ruth, U., Twarloh, B., Littot, G. C., Mulvaney, R., Röthlisberger, R., De Angelis, M., Boutron, C. F., Hansson, M., Jonsell, U., Hutterli, M. A., Lambert, F., Kaufmann, P., Stauffer, B., Stocker, T. F., Steffensen, J. P., Bigler, M., Siggaard-Andersen, M. L., Udisti, R., Becagli, S., Castellano, E., Severi, M., Wagenbach, D., Barbante, C., Gabrielli, P., and Gaspari, V.: Southern Ocean sea-ice extent, productivity and iron flux over the past eight glacial cycles, Nature, 440, 491–496, https://doi.org/10.1038/nature04614, 2006.

Yau, A. M., Bender, M. L., Robinson, A., and Brook, E. J.: Reconstructing the last interglacial at summit, greenland: insights from gisp2, Proceedings of the National Academy of Sciences, 113, 9710–9715, https://doi.org/10.1073/pnas.1524766113, 2016.

Zou, H., Sime, L. C., Bertler, N. A., Keller, E. D., and Wolff, E. W.: Plausible last interglacial Antarctic ice sheet changes do not fully explain Antarctic ice core water isotope records, Geophysical Research Letters, 52, e2024GL110 657, 2025.